

# Certifiably Correct Range-Aided SLAM

Alan Papalia, Andrew Fishberg, Brendan W. O’Neill, Jonathan P. How,  
David M. Rosen, John J. Leonard

arXiv:2302.11614v2 [cs.RO] 19 Sep 2023

**Abstract**—We present the first algorithm to efficiently compute certifiably optimal solutions to range-aided simultaneous localization and mapping (RA-SLAM) problems. Robotic navigation systems increasingly incorporate point-to-point ranging sensors, leading to state estimation problems in the form of RA-SLAM. However, the RA-SLAM problem is significantly more difficult to solve than traditional pose-graph SLAM: ranging sensor models introduce non-convexity and single range measurements do not uniquely determine the transform between the involved sensors. As a result, RA-SLAM inference is sensitive to initial estimates yet lacks reliable initialization techniques. Our approach, certifiably correct RA-SLAM (CORA), leverages a novel quadratically constrained quadratic programming (QCQP) formulation of RA-SLAM to relax the RA-SLAM problem to a semidefinite program (SDP). CORA solves the SDP efficiently using the Riemannian Staircase methodology; the SDP solution provides both (i) a lower bound on the RA-SLAM problem’s optimal value, and (ii) an approximate solution of the RA-SLAM problem, which can be subsequently refined using local optimization. CORA applies to problems with arbitrary pose-pose, pose-landmark, and ranging measurements and, due to using convex relaxation, is insensitive to initialization. We evaluate CORA on several real-world problems. In contrast to state-of-the-art approaches, CORA is able to obtain high-quality solutions on all problems despite being initialized with random values. Additionally, we study the tightness of the SDP relaxation with respect to important problem parameters: the number of (i) robots, (ii) landmarks, and (iii) range measurements. These experiments demonstrate that the SDP relaxation is often tight and reveal relationships between graph rigidity and the tightness of the SDP relaxation.

**Index Terms**—Certifiable Perception, Range-Aided SLAM, Semidefinite Programming, Riemannian Staircase

## I. INTRODUCTION

Reliable range-aided simultaneous localization and mapping (RA-SLAM) algorithms are critical to enabling autonomous navigation in a variety of environments. RA-SLAM application domains span underwater [1, 2], in air [3], underground [4], and planetary [5] environments. RA-SLAM extends standard pose-graph SLAM [6, 7] with point-to-point range measurements, enabling use of a wider range of sensing modalities. Range sensing possesses notable advantages: measurements often have known data-association, a primary failure mode

This work was partially supported by ONR grant N00014-18-1-2832, ONR MURI grant N00014-19-1-2571, the MIT-Portugal program, the National Defense Science and Engineering Graduate fellowship, and the Tillman Scholar program. Additionally, this material is based upon work supported in part by the Department of Energy/National Nuclear Security Administration under Award Number(s) DE-NA0003921, and by the Under Secretary of Defense for Research and Engineering under Air Force Contract No. FA8702-15-D-0001 with MIT Lincoln Laboratory.

Alan Papalia, Andrew Fishberg, Brendan O’Neill, Jonathan P. How, and John J. Leonard are with the Massachusetts Institute of Technology, Cambridge, MA 02139, USA, (e-mail: apapalia@mit.edu; fishberg@mit.edu; oneillb@mit.edu; jhow@mit.edu; jleonard@mit.edu)

David M. Rosen is with Northeastern University, Boston, MA 02115, USA, (email: d.rosen@northeastern.edu)

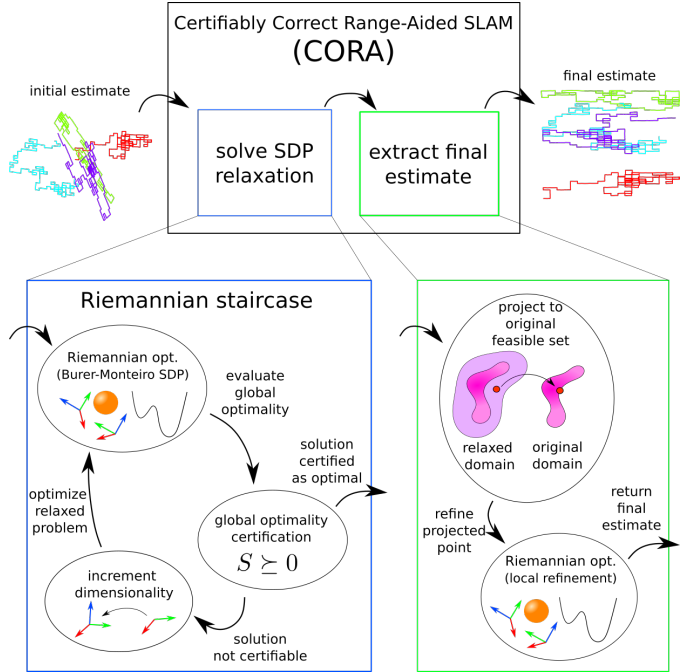


Fig. 1. A schematic overview of the proposed algorithm on a four robot RA-SLAM problem. (Top) the high-level flow, which, given an initial estimate, solves a semidefinite program (SDP) relaxation of the RA-SLAM problem. As the SDP solution is not necessarily feasible for the RA-SLAM problem, a final estimate to the original problem is then extracted and returned. (Bottom-Left) The Riemannian Staircase methodology used to solve the SDP, in which optimization is performed over increasingly lifted Riemannian optimization problems until a certified solution to the SDP is found. The Riemannian optimization is over a product manifold involving orthonormal frames and vectors on the unit-sphere, certification involves evaluating positive semidefiniteness of a specific matrix, and lifting is equivalent to increasing the dimensions of the product manifold. (Bottom-Right) extracting the final estimate via feasible set projection followed by Riemannian optimization.

of modern navigation systems [7], and in many environments (e.g., underwater) range measurements are critical to long-duration state estimation. Despite RA-SLAM’s broad applicability and the advantages of range sensing, RA-SLAM approaches lack the optimality guarantees and robustness to initialization found in modern pose-graph SLAM [8].

The difficulties surrounding RA-SLAM arise from the structure of the *maximum a posteriori* (MAP) estimation problem, which leads to a nonlinear least-squares (NLS) problem [9, 10]. As the NLS formulation is non-convex, standard approaches only guarantee locally optimal solutions and cannot distinguish local from global optimality. While these issues have been circumvented in pose-graph SLAM [8], range measurements take a fundamentally different form than pose measurements in the MAP problem which prevents application of existing techniques.

This work presents CORA, an algorithm capable of returning certifiably optimal estimates to the RA-SLAM problem.

CORA solves an SDP relaxation of the RA-SLAM problem to obtain (i) a lower bound on the optimal value of and (ii) an approximate solution to the original RA-SLAM problem. This is made possible by a novel reformulation of the RA-SLAM problem into a quadratically constrained quadratic program (QCQP), which then leads a natural SDP relaxation [11]. We demonstrate how to apply the Riemannian Staircase approach [12, 13] to obtain a solution to the SDP relaxation. The resulting SDP solution is projected to the feasible set of the original RA-SLAM problem and locally optimized to produce a final estimate. The difference between the cost of this final estimate and the SDP lower bound provides an upper bound on the solution suboptimality.

We evaluate CORA’s performance on a range of real-world RA-SLAM datasets, including a 3D aerial drone data set collected as part of this work. We show that, unlike existing approaches which often perform well but are susceptible to poor initialization and local optima, CORA consistently obtains high-accuracy solutions regardless of initialization. Additionally, we characterize the quality of the SDP lower bound and perform parameter sweeps to observe how common parameters (e.g., number of distinct robots) in RA-SLAM problems affect the tightness (the minimum attainable suboptimality gap) of the proposed SDP relaxation. While the relaxation’s tightness may not affect the quality of the final estimate, it affects the ability to obtain a certifiably optimal solution to the unrelaxed problem. This parametric study provides insight into the structure of RA-SLAM problems and suggests which characteristics lead to more difficult optimization problems.

We summarize the contributions of this paper as follows:

- The first RA-SLAM algorithm capable of producing certifiably optimal estimates.
- A parametric study of tightness of the proposed SDP relaxation.
- An open-source implementation, including all experimental data presented in this paper<sup>1</sup>.

## II. RELATED WORKS

Certification in robotic perception typically describes a certificate of optimality of some estimated quantity, where the estimation procedure is defined as an optimization problem [15, 16, 17]. Works in certifiable estimation generally are either (i) an optimizer paired with a global optimality certification scheme or (ii) an exhaustive search approach. A notable subset of the former class of works falls under *certifiably correct* methods, which can efficiently recover *provably* optimal solutions to a problem within a given problem regime [16].

### A. Sufficient Conditions for Global Optimality

Many certification schemes leverage relationships between quadratically constrained quadratic programs (QCQPs) and SDPs to construct certifiers based on Lagrangian duality. These certifiers establish sufficient conditions for optimality which, if satisfied, guarantee global optimality [17, 18, 19].

<sup>1</sup><https://github.com/MarineRoboticsGroup/cora>

Additionally, works in certification can be separated by the estimation methodology proposed; works typically pair a certifier with a local-optimizer or a SDP relaxation. The SDP approaches solve a relaxation of the original problem and then project the relaxed solution to the feasible set of the original problem. Notable SDP-based works [8, 20] established conditions when such guarantees exist. Importantly, unlike local optimization, the estimates from SDP methods are initialization-independent.

*Local-optimization and Verification:* KKT-based sufficient conditions were derived from various QCQPs and paired with local optimizers to solve problems in point-cloud registration [21, 22], multi-view geometry [23], pose-graph SLAM [24, 25], and range-only localization [26]. In addition to KKT-based certificates, a number of computer vision works developed certification schemes based on proving problem convexity over the feasible set [27, 28, 29].

*SDPs and Interior Point Methods:* Many approaches in robotic perception formulate problems as a QCQP, solve an SDP relaxation of the QCQP [30], and then project the SDP solution to the feasible set of the original problem. Often the SDP relaxation is exact, and thus the projection is a certifiably optimal solution to the original problem. Previous approaches applied standard SDP solvers to problems in geometric registration [31, 32, 33], robust point-cloud registration [34], relative pose estimation [35, 36], triangulation [37], anonymous bearing-only multi-robot localization [38], essential matrix estimation [39], pose-graph SLAM [40], and sensor calibration [41]. While standard interior point methods scale poorly for large problems, these approaches are successful on small problems and can use a broad set of solvers.

*SDPs and the Riemannian Staircase:* SDP relaxations of robotic perception problems typically admit low-rank solutions. A growing body of work applies the Riemannian Staircase methodology [12, 13] to leverage this low-rank structure and more efficiently solve the SDP. Riemannian Staircase approaches differ from the previously mentioned interior point methods in that they (i) optimize over a series of lower-dimension, non-convex, rank-restricted SDPs to solve the original SDP and (ii) these methods leverage the fact that the feasible sets of these rank-restricted problems take the form of simple manifolds, enabling the use of Riemannian optimization methods to improve optimizer performance. While the approach of solving a series of rank-restricted SDPs can *in principle* be applied to all SDPs [14, 17, 42], usage of Riemannian optimization depends on specific problem structure and does not apply to all SDPs. Within robotics, the Riemannian Staircase has been applied to pose-graph SLAM [8, 43, 44] and range-only localization [45].

*Placement of this Work:* This work falls under the Riemannian Staircase class of works. We present a SDP formulation, certification procedure, Riemannian Staircase methodology, and means for extracting an RA-SLAM estimate from a minimizer of the SDP. Our work differs from recent, important papers in certification for the closely related problem of range-only localization [26, 45], as a novel problem formulation and certification methodology were necessary to account for pose variables. Our certification approach builds upon the

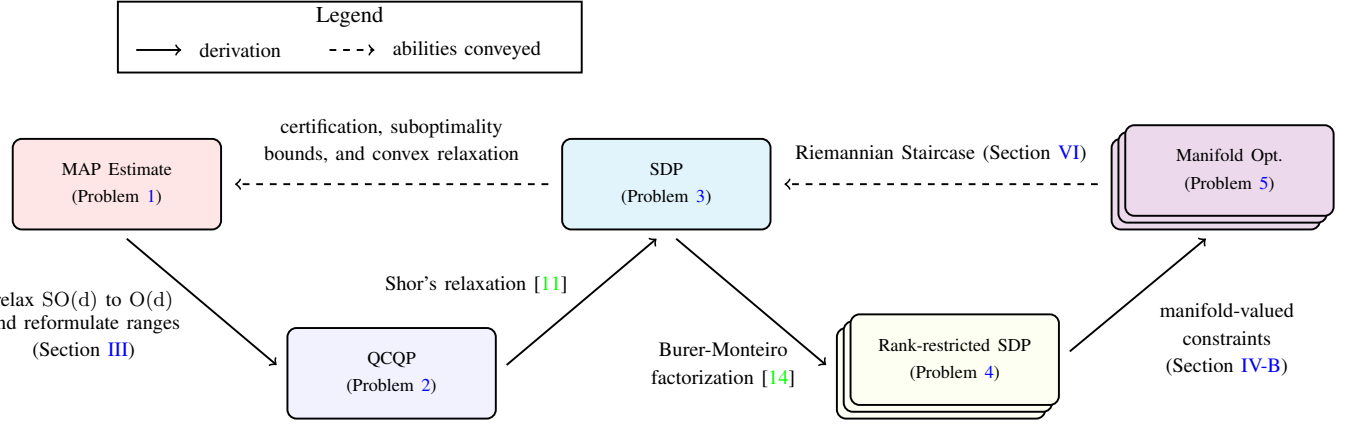


Fig. 2. **Overview of the problems stated in this paper.** We summarize how each problem is derived from the preceding problem (solid arrows) and the abilities conveyed by each problem with respect to previous problems (dashed arrows). *Derivations:* From the MAP formulation of RA-SLAM (Problem 1), we derive a QCQP relaxation (Section III). The QCQP admits a relaxation to an SDP (Problem 3) via Shor's relaxation [11]. The SDP can be solved as a series of rank-restricted SDPs (Problem 4) via the Burer-Monteiro method [14], which allows for computationally tractable solution of large-scale SDPs. Furthermore, by recognizing the manifold structure of the rank-restricted SDP constraints, the rank-restricted SDPs can be equivalently solved as manifold optimization problems (Problem 5). *Abilities conveyed:* As the SDP is a relaxation of the MAP problem, it provides means for: (i) certifying optimality of the MAP estimate, (ii) bounding the suboptimality of a MAP estimate, and (iii) an initialization-independent approach to obtaining MAP estimates. As we can determine whether a rank-restricted SDP solves the SDP (Section V) and the rank-restricted SDPs can be posed as manifold optimization problems, we can efficiently solve the SDP via the Riemannian Staircase methodology (Section VI).

KKT-based analyses of [17, 18]. Additionally, our problem formulation and estimation procedure generalize similar, key works in range-only localization [45] and pose-graph SLAM [8, 43] to the case of RA-SLAM.

### B. Exhaustive Search

Exhaustive search approaches largely use either polynomial root finding or branch-and-bound (BnB) techniques to guarantee a globally optimal solution will be found [46, 47]. Such *a priori* guarantees typically cannot be made for other approaches. These approaches come at increased computational cost, particularly as problem sizes increase.

Polynomial solving via Gröbner basis computation was applied to multi-view geometry [48, 49] and range-only localization [50]. Similarly, [51] solved a polynomial system via eigendecomposition to estimate relative camera pose.

BnB was applied to consensus maximization in rotation search [52] and special Euclidean registration [53]. [54] linearly approximated SO(3) to solve pose estimation as a mixed-integer convex program for improved BnB efficiency. Similarly, [55] integrated the iterative closest point solver into a BnB framework to efficiently perform point cloud registration. BnB was also applied to the estimation of: camera focal length and relative rotation [56], correspondence-free relative pose [57, 58], essential matrices [59, 60], and triangulation [61].

### III. RA-SLAM AS AN SDP

The RA-SLAM problem aims to estimate a collection of robot poses and beacon locations from a set of relative pose and range measurements between these poses and beacons. In this section we demonstrate how the *maximum a posteriori* (MAP) formulation of the RA-SLAM problem can be used to derive a novel SDP. This SDP underpins many of the key properties of this work. We outline the derivation of the SDP and the properties it provides in Fig. 2.

### A. MAP formulation of RA-SLAM

The MAP formulation is based on generative measurement models with Langevin distributed rotational noise [62] and Gaussian distributed translational and ranging noise:

$$\tilde{R}_{ij} = \underline{R}_{ij} R_{ij}^{\epsilon}, \quad R_{ij}^{\epsilon} \sim \text{Langevin}(I_d, \kappa_{ij}) \quad (1)$$

$$\tilde{t}_{ij} = \underline{t}_{ij} + t_{ij}^{\epsilon}, \quad t_{ij}^{\epsilon} \sim \mathcal{N}(0, \tau_{ij}^{-1} I_d) \quad (2)$$

$$\tilde{r}_{ij} = \|\underline{t}_i - \underline{t}_j\|_2 + r_{ij}^{\epsilon}, \quad r_{ij}^{\epsilon} \sim \mathcal{N}(0, \sigma_{ij}^2) \quad (3)$$

where  $\tilde{R}_{ij}, \tilde{t}_{ij}, \tilde{r}_{ij}$  are noisy relative rotational, translational, and range measurements. Similarly,  $\underline{R}_{ij}, \underline{t}_{ij}, \underline{r}_{ij}$  are the true relative rotations, translations, and ranges. Finally,  $R_{ij}^{\epsilon}, t_{ij}^{\epsilon}, r_{ij}^{\epsilon}$  represent the noisy perturbations to the measurements where the coefficients  $\kappa_{ij}$ ,  $\tau_{ij}$ , and  $(1/\sigma_{ij}^2)$  are, respectively, the rotational, translational, and ranging measurement precisions.

From the measurement models of Eqs. (1) to (3) the MAP formulation of RA-SLAM is as follows [63],

**Problem 1** (MAP formulation of RA-SLAM). *Given relative pose measurements,  $\{\tilde{R}_{ij}, \tilde{t}_{ij}\}_{(i,j) \in \mathcal{E}_p}$ , and distance measurements,  $\{\tilde{r}_{ij} \in \mathbb{R}\}_{(i,j) \in \mathcal{E}_r}$ , find the variables,  $\{R_i, t_i\}_{i=1}^n$ , which solve*

$$\begin{aligned} \min_{\substack{R_i \in \text{SO}(d) \\ t_i \in \mathbb{R}^d}} \quad & \sum_{(i,j) \in \mathcal{E}_p} \kappa_{ij} \|R_j - R_i \tilde{R}_{ij}\|_F^2 \\ & + \sum_{(i,j) \in \mathcal{E}_p} \tau_{ij} \|t_j - t_i - R_i \tilde{t}_{ij}\|_2^2 \\ & + \sum_{(i,j) \in \mathcal{E}_r} \frac{1}{\sigma_{ij}^2} (\|t_j - t_i\|_2 - \tilde{r}_{ij})^2 \end{aligned} \quad (4)$$

where  $\mathcal{E}_p$  and  $\mathcal{E}_r$  are the sets of edges representing relative pose measurements and range measurements, respectively. Additionally,  $d$  is the dimension of the problem (e.g., 2D or 3D) and  $n$  is the number of pose variables.

### B. Obtaining the SDP Relaxation

From Problem 1 we derive a relaxed problem, which takes the form of a QCQP and, in turn, leads to a convenient SDP relaxation. This QCQP (Problem 2) relaxes the special orthogonal constraint  $R_i \in \text{SO}(d)$  to an orthogonality constraint,  $R_i \in \text{O}(d)$ . This relaxation was found to have no significant impact on typical pose-graph SLAM solution quality [8, 43, 64].

Additionally, the range cost terms of Problem 1 are modified. We introduce auxiliary unit-norm vector variables,  $r_{ij} \in \mathbb{R}^d$ . This reformulation of the range cost terms in Problem 2 is equivalent to the terms presented in Problem 1 in the sense that the optimal cost and optimal translations  $t_i$  are preserved for both problems [45, Lemma 1]. This reformulation is a critical step in our approach, as it enables range measurements to be expressed in quadratic forms.

We present this relaxation in Problem 2, noting that all costs and constraints are now quadratic.

**Problem 2** (QCQP relaxation of RA-SLAM). *Given the measurements of Problem 1, find the variables,  $\{R_i, t_i\}_{i=1}^n \{r_{ij}\}_{(i,j) \in \mathcal{E}_r}$ , which solve:*

$$\begin{aligned} \min_{\substack{R_i \in \mathbb{R}^{d \times d} \\ t_i \in \mathbb{R}^d \\ r_{ij} \in \mathbb{R}^d}} \quad & \sum_{(i,j) \in \mathcal{E}_p} \kappa_{ij} \|R_j - R_i \tilde{R}_{ij}\|_F^2 \\ & + \sum_{(i,j) \in \mathcal{E}_p} \tau_{ij} \|t_j - t_i - R_i \tilde{t}_{ij}\|_2^2 \\ & + \sum_{(i,j) \in \mathcal{E}_r} \frac{1}{\sigma_{ij}^2} \|t_j - t_i - \tilde{r}_{ij} r_{ij}\|_2^2 \\ \text{subject to} \quad & R_i^\top R_i = I_d, \quad i = 1, \dots, n \\ & \|r_{ij}\|_2^2 = 1, \quad \forall (i,j) \in \mathcal{E}_r. \end{aligned} \quad (5)$$

The advantage of Problem 2 over Problem 1 is that Problem 2 is a QCQP, and therefore admits a standard SDP relaxation [11]. This SDP relaxation of Problem 2 takes the form of,

**Problem 3** (SDP relaxation of RA-SLAM). *Find  $Z \in \mathbb{R}^{k \times k}$  that solves*

$$\begin{aligned} \min_{Z \in \mathbb{R}^{k \times k}} \quad & \text{tr}(QZ) \\ \text{subject to} \quad & \text{tr}(A_i Z) = b_i, \quad i = 1, \dots, m \\ & Z \succeq 0. \end{aligned} \quad (6)$$

where  $k \triangleq n(d+1) + l$  and  $l \triangleq |\mathcal{E}_r|$  is the number of range measurements.  $Q$ , and  $A_i$  are defined in Appendices B and C.

This SDP relaxation (Problem 3) will form the basis of our approach.

## IV. SOLVING PROBLEM 3 VIA RIEMANNIAN OPTIMIZATION

While the SDP of Problem 3 is key to our approach, standard interior-point SDP solvers cannot scale application-relevant sizes of Problem 3. We derive a rank-restricted SDP from Problem 3, which substantially reduces problem dimensionality and thus computational cost. Furthermore, we

demonstrate that this specific rank-restricted SDP can be solved via Riemannian optimization, lending improved computational efficiency and insights into the geometric structure of the problem. We outline these derivations and their relationships to Problem 3 in Fig. 2.

### A. Rank-Restricted SDPs

As we expect Problem 3 to have a low-rank solution, we instead apply the Burer-Monteiro method [14, 42] to pose the problem as a rank-restricted SDP. This rank-restricted SDP reduces the problem dimensionality by substituting an assumed low-rank factorization for the optimal solution  $Z = XX^\top, X \in \mathbb{R}^{k \times p}$ , arriving at the following form:

**Problem 4** (Burer-Monteiro factorization of Problem 3). *Find  $X \in \mathbb{R}^{k \times p}$  that solves*

$$\begin{aligned} \min_{X \in \mathbb{R}^{k \times p}} \quad & \text{tr}(QXX^\top) \\ \text{subject to} \quad & \text{tr}(A_i XX^\top) = b_i, \quad i = 1, \dots, m. \end{aligned} \quad (7)$$

In this rank-restricted SDP the problem variable  $X$  is composed as follows,

$$X \in \mathbb{R}^{k \times p} \triangleq [R_1 \cdots R_n \mid r_1 \cdots r_l \mid t_1 \cdots t_n]^\top \quad (8)$$

where each element, e.g.,  $R_i \in \mathbb{R}^{p \times d}$ , can be considered a natural lifting of the variables in the QCQP of Problem 2 when  $p > d$ .

For each  $R_i \in \mathbb{R}^{p \times d}$  variable there are  $\frac{d(d+1)}{2}$  orthonormality constraints in the form of  $\text{tr}(A_i R_i^\top R_i) = b_i$ . E.g., for  $d = 2$  the constraint  $R_i^\top R_i = I_d$  can be defined by the following pairs  $(A_{jR_i}, b_j)$ :

$$\begin{aligned} A_{1R_i} &= \begin{bmatrix} 1 & 0 \\ 0 & 0 \end{bmatrix} & b_1 &= 1 \\ A_{2R_i} &= \begin{bmatrix} 0 & 1/2 \\ 1/2 & 0 \end{bmatrix} & b_2 &= 0 \\ A_{3R_i} &= \begin{bmatrix} 0 & 0 \\ 0 & 1 \end{bmatrix} & b_3 &= 1. \end{aligned}$$

Similarly, the unit-norm constraint for a single  $r_{ij}$  can be expressed as  $\text{tr}(A_{r_{ij}} r_{ij}^\top r_{ij}) = 1$ , where  $A_{r_{ij}} = [1]$ .

As these constraints all act on a single variable each, to embed them into the full state space  $\mathbb{R}^{k \times k}$  they are simply placed at the block-diagonal location corresponding to the variable they constrain. See Appendix C for further details.

In the Burer-Monteiro factorization,  $p$  constrains the rank of the solution to Problem 4, as  $\text{rank}(X) = \text{rank}(XX^\top) \leq p$ . Indeed, the rank-restricted SDP of Problem 4 is equivalent to the QCQP of Problem 2 when  $p = d$ . It follows that incrementing  $p$  provides an interpretable means of relaxing Problem 4 by increasing the allowable rank of the solution.

This relaxation methodology is key to our approach. We often need to relax the problem to escape local minima of the rank-restricted SDP but we can typically find solutions to the SDP of Problem 3 at relaxations  $p \ll k$ .

### B. Problem 4 as Riemannian Optimization

The feasible set of the rank-restricted SDP in Problem 4 can be described as a product of Riemannian manifolds.

We have established that the constraints of Problem 4 are equivalent to  $R_i^\top R_i = I_d$  for all  $R_i \in \mathbb{R}^{p \times d}$  and  $\|r_{ij}\|_2^2 = 1$  for all  $r_{ij} \in \mathbb{R}^p$ . The orthonormal constraint,  $R_i^\top R_i = I_d$  is equivalent to the Stiefel manifold  $\text{St}(p, d)$  [8]. Similarly, the unit-norm constraints,  $\|r_{ij}\|_2^2 = 1$ , are equivalent to  $S^{p-1}$ , the unit-sphere in  $\mathbb{R}^p$ . Thus the feasible set of Problem 4 can be expressed as the product of Riemannian manifolds for any  $p$ .

Recognizing this Riemannian structure to our problem (i) allows us to apply mature Riemannian optimization techniques to solve the rank-restricted SDPs and (ii) provides insights into the smoothness of the underlying constraints which will prove useful in our certification methodology. We describe the corresponding Riemannian optimization problem in Problem 5.

**Problem 5** (Problem 4 as Riemannian optimization). *Given the measurements of Problem 1, find the variables,  $\{R_i, t_i\}_{i=1}^n \cup \{r_{ij}\}_{(i,j) \in \mathcal{E}_r}$ , which solve:*

$$\begin{aligned} \min_{\substack{R_i \in \text{St}(p, d) \\ t_i \in \mathbb{R}^p \\ r_{ij} \in S^{p-1}}} \quad & \sum_{(i,j) \in \mathcal{E}_p} \kappa_{ij} \|R_j - R_i \tilde{R}_{ij}\|_F^2 \\ & + \sum_{(i,j) \in \mathcal{E}_p} \tau_{ij} \|t_j - t_i - R_i \tilde{t}_{ij}\|_2^2 . \\ & + \sum_{(i,j) \in \mathcal{E}_r} \frac{1}{\sigma_{ij}^2} \|t_j - t_i - \tilde{r}_{ij} r_{ij}\|_2^2 \end{aligned} \quad (9)$$

where  $S^{p-1}$  is the unit-sphere in  $\mathbb{R}^p$ .

We emphasize that Problem 5 is exactly the rank-restricted SDP of Problem 4, reformatted to explicitly state that the feasible set of Problem 4 is a product of Riemannian manifolds.

## V. CERTIFYING RANK-RESTRICTED SDP SOLUTIONS

In this section we demonstrate how previous results in certifiable estimation [17] can be applied to the rank-restricted SDP (Problem 4) to determine whether a candidate solution  $X^*$  is globally optimal.

This globally optimality test centers around the *certificate matrix*  $S$ , which is formed from the data matrix  $Q$ , the constraint matrices  $A_i$ , and their corresponding Lagrange multipliers  $\lambda_i$  at a KKT point:

$$S \triangleq Q + \sum_{i=1}^m \lambda_i A_i. \quad (10)$$

If, given a KKT point  $X^*$  of Problem 4, we obtain an  $S$  which is positive semidefinite, then  $X^*$  solves both Problem 3 and Problem 4. This is because if  $S \succeq 0$  then  $Z = XX^\top$  is a KKT point of the SDP of Problem 3 and thus must be optimal. Critically, our approach to obtaining  $S$  requires that the linear independence constraint qualification (LICQ) is satisfied. In the following subsections we discuss the LICQ, prove it is satisfied for our problem, and then describe our algorithm for performing certification.

### A. The Linear Independence Constraint Qualification

The certificate matrix we devise is a function of the Lagrange multipliers  $\lambda$  at a given solution point  $X^*$ . However, to guarantee a unique set of Lagrange multipliers the LICQ must be satisfied [65]. Without a unique set of Lagrange multipliers, the optimality condition becomes a test for whether there exist *some* valid Lagrange multipliers which generate a  $S \succeq 0$ . This thus becomes a SDP feasibility problem of the same dimension as our original SDP (Problem 3) and thus is computationally intractable for desired RA-SLAM problem sizes.

The LICQ requires that the gradients of the constraints are linearly independent. For Problem 4, the LICQ is equivalent to linear independence of  $\{\nabla_X \text{tr}(A_i X X^\top), i = 1, \dots, m\}$  evaluated at  $X = X^*$ . This condition is equivalent to the following *adjoint constraint Jacobian*,

$$K \in \mathbb{R}^{(kp) \times m} \triangleq [\text{vec}(A_1 X^*) \mid \dots \mid \text{vec}(A_m X^*)] \quad (11)$$

having full column rank, where  $\text{vec}(\cdot)$  is the row-wise vectorization operator.

### B. Problem 4 satisfies the LICQ

We prove that the LICQ is satisfied for all feasible points of Problem 4. Our proof utilizes the fact that the constraints of Problem 4 are defining functions of the embedded submanifolds:  $\text{St}(p, d)$  and  $S^{p-1}$  [66, Chapter 7].

**Theorem 1.** *The LICQ is satisfied for all feasible points of Problem 4.*

*Proof:* Recall that the constraints of Problem 4 have block-diagonal sparsity patterns. Each constraint only accesses a single variable,  $R_i$  or  $r_{ij}$ . As a result, there should be an ordering of constraints and variables which results in a block-diagonal adjoint constraint Jacobian.

Without loss of generality, we define an ordering over the constraints. First group the constraints by their associated variable. We define  $\{A_{R_i}\}$  as the  $\frac{d(d+1)}{2}$  constraints associated with  $R_i$  and  $\{A_{r_{ij}}\}$  as the single constraint associated with  $r_{ij}$ . The ordering within each group is arbitrary. Furthermore, order these groups by the order of the associated variables as seen in Eq. (8).

Given this constraint ordering and the variable ordering of Eq. (8), the adjoint constraint Jacobian of Eq. (11) takes a block-diagonal form. The first  $n$  blocks are of shape  $(dp \times \frac{d(d+1)}{2})$ . These blocks are the entries associated with the constraints  $R_i^\top R_i = I_d$ . The remaining  $l$  blocks are  $(p \times 1)$  and are the entries associated with the constraints  $\|r_{ij}\|_2^2 = 1$ .

As the adjoint constraint Jacobian is block-diagonal, it is sufficient to show that each block has full column rank. This can be done by recognizing that the original constraints are defining functions of  $\text{St}(p, d)$  and the unit-sphere in  $\mathbb{R}^p$  and that each block is the Jacobian of a single defining function.

By definition, the Jacobian of the defining function of an embedded submanifold is full rank at any point on the submanifold [66, Definition 3.10]. At any feasible point of Problem 4 each low-dimensional variable (e.g.,  $R_i$ ) is satisfying its defining function and thus is on its corresponding submanifold. Therefore, at any feasible point, each block of

the adjoint constraint Jacobian  $K$  is full rank. Thus, at any feasible point the adjoint constraint Jacobian has full column rank and the LICQ is satisfied. ■

### C. Performing Certification

In this section we demonstrate how solution certification is reduced to three steps: (i) solving a single linear least-squares problem, (ii) matrix addition, and (iii) evaluating positive semidefiniteness of a real, symmetric matrix. All matrices in these computations are sparse, enabling efficient computation.

*Computing Lagrange Multipliers:* As the Lagrange multipliers are a function of the specific solution point evaluated, they must be computed for each candidate solution. By the stationarity condition of the KKT conditions, we determine the Lagrange multipliers via linear least-squares. For any stationary point, the partial derivative of the Lagrangian with respect to the problem variable is zero [67, Theorem 12.1]. Gathering the Lagrange multipliers as a vector,  $\lambda \in \mathbb{R}^m \triangleq [\lambda_1, \dots, \lambda_m]$ , the partial derivative of the Lagrangian of Problem 4 is

$$\begin{aligned} \partial_X \mathcal{L}(X, \lambda) &= \partial_X \text{tr}(QXX^\top) \\ &\quad + \partial_X \sum_{i=1}^m (\text{tr}(A_i XX^\top) - b_i) \lambda_i \\ &= 2QX + 2 \left( \sum_{i=1}^m \lambda_i A_i \right) X. \end{aligned} \quad (12)$$

It follows from Eq. (12) that the first-order stationarity condition of Problem 4 is,

$$QX^* + \left( \sum_{i=1}^m \lambda_i A_i \right) X^* = \mathbf{0}, \quad (13)$$

where  $X^* \in \mathbb{R}^{k \times p}$  is a stationary point of Problem 4 and  $\mathbf{0}$  is the zero matrix.

Observe that Eq. (13) is linear with respect to the Lagrange multipliers. We rearrange Eq. (13) to arrive at

$$\sum_{i=1}^m (A_i X^*) \lambda_i = -QX^*. \quad (14)$$

By vectorizing each side of Eq. (14) we arrive at

$$K\lambda = -\text{vec}(QX^*) \quad (15)$$

where  $K$  is the adjoint constraint Jacobian of Eq. (11). Thus, the Lagrange multipliers  $\lambda$  may be estimated by solving the linear system of Eq. (15). As the adjoint constraint Jacobian is full rank (Theorem 1), the Lagrange multipliers are uniquely determined.

*Building  $S$  and Evaluating Optimality:* Given the Lagrange multipliers and constraints,  $(\lambda_i, A_i)$ , the certificate matrix can be formed as in Eq. (10):  $S \triangleq Q + \sum_{i=1}^m \lambda_i A_i$ .

By [17, Theorem 4], if  $S \succeq 0$ , the candidate solution  $X^*$  is globally optimal. For this problem, the most efficient means of checking  $S \succeq 0$  is by attempting to Cholesky factorize  $S + \beta I$ , where  $0 < \beta \ll 1$ . Existence of a factorization ( $M = LL^\top$ ) is sufficient proof of positive semidefiniteness of  $M$  and all positive definite matrices admit a Cholesky factorization. We can thus interpret  $\beta$  as a numerical tolerance parameter for the positive semidefiniteness of  $S$ . We summarize this certification scheme in Algorithm 1.

---

**Algorithm 1** Certify Optimality of a Candidate Solution,  $X^*$ 


---

**Input:** the solution to certify  $X^* \in \mathbb{R}^{k \times p}$ , positive semidefinite tolerance parameter  $\beta \in \mathbb{R}_{++}$

**Output:** whether  $X^*$  is a low-rank solution to Problem 3

**Require:**  $X^*$  is locally optimal

```

function CERTIFY( $X^*, \beta$ )
   $\lambda \leftarrow$  solve the linear system of Eq. (15)
   $S \leftarrow Q + \sum_{i=1}^m \lambda_i A_i$ 
  try Cholesky( $S + \beta I$ )
    return certified = True
  catch  $S + \beta I$  not positive definite
    return certified = False

```

---

## VI. CERTIFIABLY CORRECT ESTIMATION

In this section we describe our approach to certifiably correct estimation. We demonstrate that the rank-restricted SDP of Problem 4 can be solved via Riemannian optimization, enabling use of the Riemannian Staircase methodology. We then describe the Riemannian Staircase as applied to Problem 4 and discuss how we use the Riemannian Staircase estimate to extract an estimate to the MAP problem (Problem 1).

### A. The Riemannian Staircase

The Riemannian Staircase approach we use follows the general methodology outlined in [12, Algorithm 1] with slight alterations. Specifically, Riemannian optimization is performed at a given level of relaxation, as determined by  $p$ . If the estimate  $X^*$  is found to be optimal (Algorithm 1) then the algorithm returns the certified solution. If  $X^*$  is not certified as optimal,  $p$  is incremented and the previous estimate is used to initialize the relaxed problem. This process continues until a certifiably optimal solution is found<sup>2</sup>.

Critically, when incrementing  $p$  the estimate will be a first-order stationary point if lifted by appending a column of zeros to  $X^*$ . We use a saddle escape technique which computes a second-order descent direction from the negative eigenspace of  $S$  to perturb the solution off the stationary point [12, 17].

The primary differences between our approach and [12, Algorithm 1] are that the previous work used rank-deficiency of the estimate to certify the solution. Our certification scheme allows for us to certify solutions which are not rank-deficient, permitting computational advantages as we can certify solutions at lower levels of relaxation. Additionally, we use a specialized eigensolver which allows us to compute the saddle escape direction typically 1-2 orders of magnitude faster than standard eigensolvers [68].

In our implementation of the Riemannian Staircase we use the Riemannian Trust-Region (RTR) method [69]. Inner iterations of the RTR method solve a trust-region subproblem via a conjugate gradient method. The computational efficiency of RTR can be highly dependent on the conditioning of this

<sup>2</sup>There are known bounds on the required  $p$  to guarantee such that every second-order critical point of Problem 4 is globally optimal for Problem 3 [13, 42]. In practice, these bounds are often well above the level of relaxation required to obtain an optimal solution to Problem 3.

---

**Algorithm 2** Certifiably Correct RA-SLAM

---

**Input:** an initial estimate of a Problem 3 solution  $X_0 \in \mathbb{R}^{k \times p}$   
**Output:** a final estimate  $X^*$ , the lower-bound obtained by solving Problem 3  $f_{sdp}$ , and the final objective value  $f_{cora}$

```

function CORA( $X_0$ )
   $\beta \leftarrow 10^{-5}$ 
   $X^* \leftarrow X_0$ 
  certified  $\leftarrow$  certify( $X^*, \beta$ )
  while not certified do
    // lift  $X^*$  by appending a column
    // of zeros and performing saddle escape
     $X^* \leftarrow$  SaddleEscape( $[X^* \ 0]$ )
     $X^*, f_{sdp} \leftarrow$  RiemannianOpt( $X^*, Q$ )  $\triangleright$  Problem 5
    certified  $\leftarrow$  certify( $X^*, \beta$ )  $\triangleright$  Algorithm 1
  end
   $X^* \leftarrow$  ProjectSolution( $X^*, d$ )  $\triangleright$  Algorithm 3
   $X^*, f_{cora} \leftarrow$  RiemannianOpt( $X^*, Q$ )
  return  $X^*$ 

```

---

subproblem. We devise a novel preconditioner for the trust-region subproblem which leverages the graph structure of the data matrix  $Q$ . See Appendix D for further details and evaluation against standard preconditioning strategies.

### B. Certifiably Correct Estimation

We have now established: a certification scheme, means for lifting the Problem 4 to higher dimensions, and how to represent each lifted relaxation of Problem 4 as a Riemannian optimization problem. We combine these three contributions to construct an initialization-independent approach to certifiably correct RA-SLAM (CORA).

Given an initial estimate  $X_0$  our Riemannian Staircase approach is applied to obtain a symmetric factor  $X^*$  for a solution of Problem 3. This SDP solution is projected to the feasible set of the original problem (Problem 1) and the projected solution is refined with local Riemannian optimization. We describe these steps in Algorithm 2.

We note that by obtaining a certifiably optimal solution to Problem 3 we also establish a lower-bound on the optimal value of Problem 1. This lower-bound both provides a means of certification, and an upper-bound on suboptimality should the SDP relaxation not be tight.

## VII. EXPERIMENTS

CORA was evaluated through a variety of real-world and simulated RA-SLAM experiments. Two classes of experiments were performed:

- 1) On a series of real-world RA-SLAM problems CORA was compared against a state-of-the-art local optimizer typically used in RA-SLAM [71]. These tests aimed to understand CORA's ability to obtain high-quality solutions, as measured by rotational and translational errors in the estimated poses. The RA-SLAM scenarios are described in Table I, with results summarized in Tables II and III and Fig. 4. (Section VII-A)

---

**Algorithm 3** Project Problem 4 Point to Feasible Set of Problem 1

---

**Input:** a feasible point to Problem 4,  $X^*$ , in the form of  $X^* = [R_1^* | \cdots | R_n^* | r_1^* | \cdots | r_l^* | t_1 \dots t_n]^\top$  and the dimension to project to  $d$

**Output:** a feasible point to Problem 1,  $X^{\text{proj}}$

```

function ProjectSolution( $X^*, d$ )
   $[U_d, S_d, V_d^\top] \leftarrow$  svd( $X^*$ )  $\triangleright$  thin SVD [70, Sec. 2.5.3]
   $X \leftarrow S_d V_d^\top \in \mathbb{R}^{d \times dn}$ 
  for  $i \in \{1, \dots, n\}$  do
    // project to SO(d) via SVD (e.g., [8, Sec. 4.2])
     $R_i^{\text{proj}} \leftarrow$  ProjectToSO( $R_i$ )
     $t_i^{\text{proj}} \leftarrow t_i$ 
  for  $i \in \{1, \dots, l\}$  do
     $r_i^{\text{proj}} \leftarrow \frac{r_i}{\|r_i\|_2}$   $\triangleright$  normalize
   $X^{\text{proj}} \leftarrow [R_1^{\text{proj}} \dots R_n^{\text{proj}} | r_1^{\text{proj}} \dots r_l^{\text{proj}} | t_1^{\text{proj}} \dots t_n^{\text{proj}}]$ 
  return  $X^{\text{proj}}$ 

```

---

- 2) A series of simulated problems were constructed with parameter sweeps of: the number of robots, the number of beacons, and the density of inter-robot range measurements. These tests were performed both with and without inter-robot relative pose measurements. The aim was to empirically evaluate the the tightness of the SDP relaxation (Problem 3) with respect to common parameters of RA-SLAM problems. (Section VII-B)

We have attempted to present a descriptive, yet concise, picture of CORA through these experiments. However, we recognize that future users may hope to understand other aspects of CORA or study CORA's performance on a specific problem class. CORA, the experimental data for all of these problems, and the tools to generate the simulated problems are available at <https://github.com/MarineRoboticsGroup/cora>.

### A. Real-world Evaluation

We compare the trajectories obtained by CORA on a series of real-world RA-SLAM scenarios. The 3D aerial drone scenario is a new dataset that was collected in the course of this work and is described in Section VII-A1. The remaining scenarios are taken from the literature [72, 73]. We summarize the experiments in Table I.

The trajectory is evaluated by comparison to ground truth. The translational and rotational errors between the estimated and ground truth trajectories are computed by evo [74].

For each scenario, we compare the trajectory obtained by CORA to a variety of baselines. Each baseline uses the GTSAM Levenberg-Marquardt optimizer [71] to refine a given initialization. As initialization requirements differ in the single- and multi-robot cases due to the need to estimate the relative pose between robots, we consider additional initialization strategies for the multi-robot case. The strategies we compare against represent a range of realistic initialization approaches, depending on the information available to the user. In all cases, CORA was initialized randomly to demonstrate its initialization-independence.

Scenario	# Robots	# Beacons	Odometry	Ranging	Reference
3D Aerial Drone	1	1	Visual	UWB	Section VII-A1
2D Ground Vehicle (Plaza [72])	1	4	Inertial + Wheel	UWB	[72]
2D Ground Vehicles (TIERS [73])	4	1	Visual	UWB	[73]

TABLE I

OVERVIEW OF REAL-WORLD EXPERIMENTS: THE REAL-WORLD SCENARIOS USED TO EVALUATE CORA. WE DESCRIBE THE NUMBER OF ROBOTS AND BEACONS, THE ODOMETRY AND RANGING SENSORS USED, AND A REFERENCE FOR FURTHER DETAILS.



Fig. 3. **Drone experiment equipment:** The hexcopter and ground-station used in our drone experiment.

The *single-robot* initialization strategies are: (i) SCORE, a state-of-the-art initialization strategy for RA-SLAM [63], (ii) ground-truth beacon positions (GT), and (iii) random beacon positions (R). In cases (ii) and (iii), the first poses are taken as ground truth and following poses are initialized via odometry.

In the *multi-robot* case, we consider the following initialization strategies: (i) SCORE, (ii) ground-truth starting poses and beacon positions (GT-GT), (iii) ground-truth starting poses and random beacon positions (GT-R), (iv) random starting poses and ground-truth beacon positions (R-GT), and (v) random starting poses and random beacon positions (R-R). In cases (ii) - (v), for each robot, every pose after the first is initialized via odometry.

The corresponding error metrics are shown in Tables II and III and plotted in Fig. 4. These results are discussed in Section VII-A2. We present visualizations of the estimated trajectories in Appendix Section A in Figs. 6 to 8.

1) *Drone Experiments:* We present experiments with a hexcopter drone, equipped with six Nooploop ultra-wideband (UWB) radios and an Intel RealSense D435i camera, and a static ground station with four Nooploop UWB radios. The UWB sensors were used for two-way time-of-flight range estimation. Ground truth for the drone and ground station were obtained from a motion capture system.

Odometry measurements were extracted from camera images via Kimera-VIO [75]. The drone was flown in two rectangular paths over a 10 meter by 10 meter area at a constant height. A single range measurement between the drone and ground-station was extracted at 10 Hz by averaging over all measurements obtained between the drone and ground-station since the previous measurement. Analysis of this measurement extraction approach showed that the resulting measurements were accurate measurements of the range between the center of the drone and the center of the ground-station.

2) *Discussion of Real-World Experiments:* In all of the experiments CORA obtained a trajectory which was qualitatively correct despite being initialized with random values. This is supported by the errors shown in Fig. 4; in each case CORA

obtained errors which were either lowest, or were comparable to the lowest error baseline.

In contrast to CORA, the GTSAM baselines demonstrated a strong dependence on initialization to obtain correct solutions. Notably, in the single-drone experiment, the baseline which used an initial estimate with the ground truth beacon position (GT) obtained a clearly suboptimal estimate. Furthermore, as expected, the single-robot baselines which used randomly initialized beacon positions (R) typically obtained low-quality estimates.

On the multi-robot, single-beacon TIERS data set, CORA obtained a trajectory identical to those estimated with ground truth starting poses (GT-GT and GT-R). As the TIERS data set has notably high-quality odometry, state estimation with ground truth initial poses is nearly the same as localizing the single beacon from a large number of range measurements. As suggested by the large errors obtained by the baselines which do not use ground truth initial poses (SCORE, R-GT, and R-R) the problem is substantially more challenging without ground truth initial poses, as the relative poses between different robots must be estimated entirely from the range measurements. However, CORA obtained a high-quality estimate from a random initialization, highlighting (i) its initialization-independence and (ii) ability to solve challenging RA-SLAM problems.

### B. Tightness of the SDP Relaxation

We perform a series of parameter sweeps in a 2-D simulated environment to evaluate the tightness of the SDP relaxation (Problem 3) with respect to common parameters of RA-SLAM problems. As we cannot *in general* guarantee that we are obtaining an optimal solution to the MAP problem (Problem 1), we attempt to evaluate the tightness of the SDP relaxation through the optimality gap  $f_{\text{cara}} - f_{\text{sdp}}$ , where  $f_{\text{cara}}$  is the objective value of the final solution obtained by CORA and  $f_{\text{sdp}}$  is the objective value of the SDP solution. This optimality gap is an upper bound on the gap between the optimal solution to the MAP problem and the SDP solution and thus serves as a proxy for the tightness of the SDP relaxation. To account for differences in scale between objective values of different problems, we instead report the relative optimality gap  $\frac{f_{\text{cara}} - f_{\text{sdp}}}{f_{\text{sdp}}}$ .

The parameter sweeps are over: the number of robots, the number of beacons, and the density of inter-robot range measurements. For each parameter value we generate 20 random instances.

Additionally, we perform parameter sweeps both with and without inter-robot relative pose measurements (inter-robot

TABLE II

**REAL-WORLD, SINGLE-ROBOT RESULTS:** THE ERROR OF THE TRAJECTORIES ESTIMATED BY CORA AND GTSAM ON SINGLE-ROBOT REAL-WORLD DATASETS. THE INITIALIZATION COLUMN INDICATES HOW THE OPTIMIZATION WAS INITIALIZED, WITH OPTIONS BEING: SCORE [63], GROUND-TRUTH BEACON POSITIONS (GT), OR RANDOM BEACON POSITIONS (R). FOR GTSAM (GT) AND GTSAM (R) POSES WERE INITIALIZED VIA ODOMETRY.

Initialization	3D Aerial Drone		Plaza 1 [72]		Plaza 2 [72]	
	SCORE [63]	GT Beacon Positions	Rot. RMSE (deg) ↓	Tran. RMSE (meter) ↓	Rot. RMSE (deg) ↓	Tran. RMSE (meter) ↓
CORA (Ours)			7.96	<b>0.54</b>	1.40	0.29
GTSAM (SCORE)	✓		<b>4.95</b>	0.70	<b>1.05</b>	<b>0.25</b>
GTSAM (GT)		✓	53.44	1.84	<b>1.05</b>	<b>0.25</b>
GTSAM (R)			78.76	3.54	15.97	32.40
CORA (Ours)			1.58	<b>0.27</b>		
GTSAM (GT)			9.04	0.31		
GTSAM (R)			9.04	0.31		

TABLE III

**REAL-WORLD, MULTI-ROBOT RESULTS:** THE ERROR OF THE TRAJECTORIES ESTIMATED BY CORA AND GTSAM ON THE TIERS DATASET [73]. THE INITIALIZATION COLUMN INDICATES HOW THE OPTIMIZATION WAS INITIALIZED. IN ADDITION TO SCORE [63], OPTIONS VARIED BY WHETHER THE STARTING POSES OF EACH ROBOT AND BEACON POSITION WERE TREATED AS KNOWN. IF KNOWN, THE STARTING POSE AND/OR BEACON POSITION WAS INITIALIZED AT THE GROUND TRUTH POSITION. OTHERWISE, THE STARTING POSE AND/OR BEACON POSITION WAS INITIALIZED RANDOMLY. ALL SUBSEQUENT POSES WERE INITIALIZED VIA ODOMETRY.

Initialization	TIERS [73]				
	SCORE [63]	GT Starting Pose	GT Beacon Position	Rot. RMSE (deg) ↓	Tran. RMSE (meter) ↓
CORA (Ours)				<b>2.29</b>	<b>0.04</b>
GTSAM (SCORE)	✓			88.90	6.54
GTSAM (GT-GT)		✓	✓	<b>2.29</b>	<b>0.04</b>
GTSAM (GT-R)		✓		<b>2.29</b>	<b>0.04</b>
GTSAM (R-R)				104.98	10.93
GTSAM (R-GT)			✓	106.91	9.51

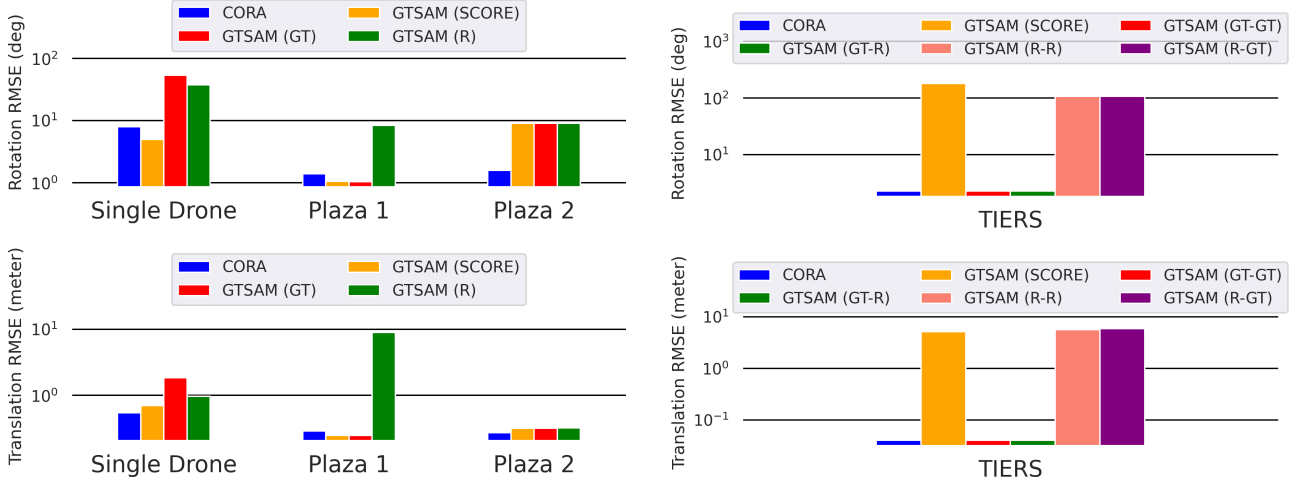


Fig. 4. **Trajectory errors across the real-world experiments.** The root-mean-square error (RMSE) of the estimated trajectories are computed, with translational and rotational components treated separately. The left and right plots respectively show results for single-robot and multi-robot experiments. In each plot, the trajectory errors of CORA (blue) are compared to GTSAM with various initialization strategies (see descriptions in Tables II and III).

loop closures). This allows us to understand the impact of the underlying pose-graph component on the tightness of the SDP relaxation. We motivate this study by framing the RA-SLAM problem as the combination of pose-graph optimization (estimation of nodes connected by relative pose measurements) and range-based localization (estimation of nodes connected by range measurements). As the SDP relaxation of pose-graph optimization is often tight as long as the underlying graph is connected [8, 20], one may wonder whether the SDP relaxation of RA-SLAM is tight in the case that the underlying pose-graph optimization component is connected.

We list the values of our parameter sweep in Table IV.

For each parameter sweep the default value is used for all parameters except the one being swept. Each instance consisted of 4000 robot poses. The experiments with inter-robot loop closures were performed with 200 inter-robot loop closures.

We show the obtained optimality gaps in Fig. 5, which demonstrate that in the case of inter-robot loop closures the attainable relative optimality gap is consistently less than 0.2%. In the case without inter-robot loop closures, the relative optimality gap is typically less than 10%. This still suggests that the SDP relaxation is sufficiently tight to be useful, but that without inter-robot loop closures the SDP relaxation is not

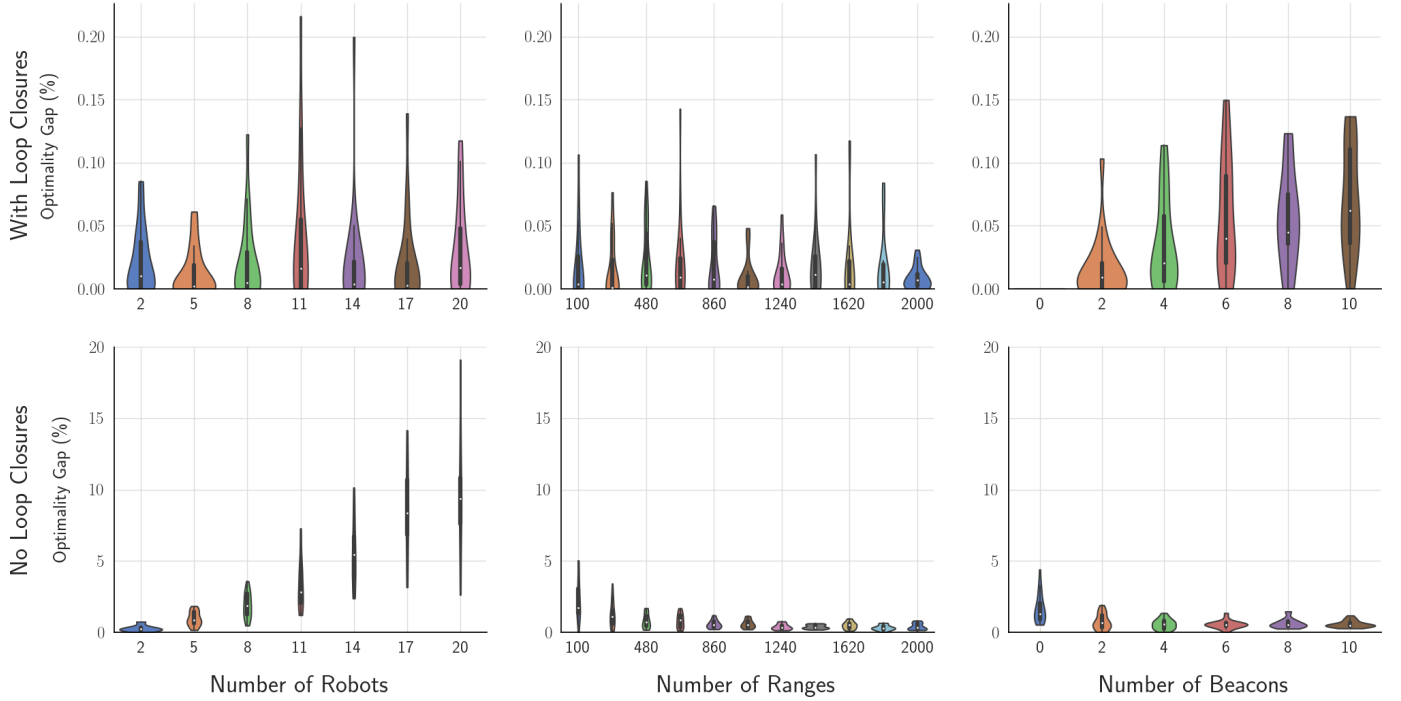


Fig. 5. **Empirical evaluation of relative suboptimality gap.** Note that the y-axis is in units of percent and that the scale of the upper row is two orders of magnitude less than the lower row. The relative suboptimality gap obtained by CORA on a series of simulated parameter sweeps as described in Section VII-B. Each parameter value was repeated 20 times; violin plots with strict cutoff at the minimum and maximum values are shown. (Top) the suboptimality gap for the parameter sweeps in which 200 inter-robot relative pose measurements (loop closures) were included in the problem. The case with inter-robot loop closures and no beacons is not visible because all instances had zero relative optimality gap. (Bottom) the suboptimality gap for the parameter sweeps in which no inter-robot relative pose measurements were included.

TABLE IV  
PARAMETER SWEEP VALUES FOR SIMULATED EXPERIMENTS

Parameter	Default Value	Sweep Range
Number of Robots	4	2–20
Number of Beacons	2	0–10
Number of Ranges	500	100–2000

exactly tight. These results suggest that the rigidity introduced by inter-robot loop closures plays a substantial role in the tightness of the SDP relaxation.

In Table V we show the percentage of experiments with relative optimality gap less than  $10^{-5}$ , which we consider to be within numerical tolerance of zero. As can be seen, many of the experiments with inter-robot loop closures (over 30%) had zero relative optimality gap. In contrast, only a small fraction of the experiments without inter-robot loop closures (on the order of 1%) had zero relative optimality gap. This suggests that while the proposed relaxation may be tight both with and without loop closures, the presence of loop closures can greatly strengthen the tightness of the relaxation.

This hypothesis on the connection between the tightness of the SDP relaxation and the rigidity of the underlying pose-graph component is further supported by the parameter sweeps over the number of robots and the number of beacons.

With increasing numbers of robots, the relative optimality gap only appeared to increase in the scenario lacking inter-robot loop closures. This is likely because when lacking inter-robot loop closures, each additional robot adds unconstrained degrees of freedom to the underlying pose-graph.

TABLE V  
PERCENTAGE OF SIMULATED EXPERIMENTS WITH ZERO SUBOPTIMALITY.  
WE CONSIDER THE OPTIMALITY GAP TO BE ZERO IF THE RELATIVE  
OPTIMALITY GAP IS LESS THAN  $10^{-5}$ .

Parameter	% Experiments with Zero Suboptimality	
	With Loop Closures	Without Loop Closures
Number of Robots	36.2%	0.7%
Number of Ranges	33.3%	0.5%
Number of Beacons	31.0%	3.4%

Interestingly, the addition of beacons appeared to have differing effects in the cases with and without inter-robot loop closures. With loop closures, the relative optimality gap appeared to increase slightly as the number of beacons increased. Notably, with no beacons all problems were solved to zero suboptimality. This is likely because the beacons introduced additional degrees of freedom which were not constrained by relative pose measurements and thus added potential symmetry or ambiguity to the solution. In contrast, the addition of beacons appeared to decrease the relative optimality gap in the case without inter-robot loop closures. We hypothesize this is because the beacons improved the underlying graph connectivity and thus helped to better constrain the relative poses of the robots.

Addition of range measurements appeared to have no discernable effect in the case with inter-robot loop closures. This is likely because the loop closures sufficiently constrain the relative poses of the robots. In contrast, without loop closures, the addition of range measurements appeared to

tighten the relaxation and result in a decrease in the relative optimality gap. This is likely because, similar to the case of adding beacons, the range measurements improved the graph connectivity such that increasing the number of measurements better constrained the relative poses of the robots.

We would like to emphasize that while the SDP relaxation is likely not exactly tight for many RA-SLAM problems, the experiments and results presented in this section suggest that the SDP relaxation is sufficiently tight to be useful in practice. We view the observation that the SDP relaxation is not exactly tight as a point of theoretical interest and motivation for future work, rather than as a substantial limitation of the SDP relaxation.

### VIII. CONCLUSION

In this work we described CORA, the first algorithm to obtain certifiably optimal RA-SLAM solutions. CORA combines two novel algorithmic capabilities for RA-SLAM, (i) a global optimality certification method and (ii) a Riemannian Staircase methodology for initialization-independent certifiably correct RA-SLAM.

We demonstrated the efficacy of CORA on a series of real-world experiments. We demonstrated that, unlike existing approaches, which often perform well but are susceptible to poor initialization and local optima, CORA is initialization-independent and consistently obtains low-error estimates.

Additionally, we studied the tightness of the SDP relaxation which underlies many of CORA's capabilities. We found that under many realistic conditions the SDP relaxation is tight (i.e., the relative suboptimality gap is below  $10^{-5}$ ). Furthermore, in conditions where the SDP relaxation likely is not tight we still typically obtain relative suboptimality gaps below 10%, suggesting that the SDP relaxation is sufficiently tight to be practically useful.

Our parametric study of SDP tightness pointed to a strong relationship between the rigidity of the pose-graph component of the RA-SLAM problem and the tightness of the SDP relaxation. This empirical observation suggested that a fully-connected pose-graph component has a strong effect on the tightness of the SDP relaxation. Additionally, this study suggested that in the absence of a fully-connected pose-graph component the addition of range measurements and static beacons can substantially improve the tightness of the SDP relaxation. We view further theoretical study of these relationships as promising future work.

### IX. DISCLAIMER

This report was prepared as an account of work sponsored by an agency of the United States Government. Neither the United States Government nor any agency thereof, nor any of their employees, makes any warranty, express or implied, or assumes any legal liability or responsibility for the accuracy, completeness, or usefulness of any information, apparatus, product, or process disclosed, or represents that its use would not infringe privately owned rights. Reference herein to any specific commercial product, process, or service by trade

name, trademark, manufacturer, or otherwise does not necessarily constitute or imply its endorsement, recommendation, or favoring by the United States Government or any agency thereof. The views and opinions of authors expressed herein do not necessarily state or reflect those of the United States Government or any agency thereof.

### APPENDIX A VISUALIZATION OF REAL-WORLD TRAJECTORIES

We provide visualizations of the estimated trajectories from the real-world experiments in Figs. 6 to 8. As can be seen, and is described in the main text, the trajectories estimated by CORA are highly accurate.

In general, both CORA and GTSAM are capable of obtaining high-quality estimates. However, there are several cases where GTSAM fails to obtain a high-quality estimate, despite reasonable initializations. These are the scenarios in which CORA provides practical advantage, as CORA does not depend on the quality of the initialization.

### APPENDIX B FORM OF THE DATA MATRIX, $Q$

$Q$  is a sparse, real, symmetric, positive-semidefinite matrix which encodes the cost of the RA-SLAM problem. We describe  $Q$  as the summation of the relative-pose cost terms ( $Q_p$ ) with the range cost terms ( $Q_r$ ), i.e.,

$$Q \triangleq Q_p + Q_r \quad (16)$$

$$Q_p \triangleq \begin{bmatrix} L(G^p) + \Sigma & 0 & \tilde{V} \\ 0 & 0 & 0 \\ \tilde{V}^\top & 0 & L(G^r) \end{bmatrix} \quad (17)$$

$$Q_r \triangleq \begin{bmatrix} 0 & 0 & 0 \\ 0 & W\tilde{D}^2 & \tilde{D}WC \\ 0 & C^\top W\tilde{D} & C^\top WC \end{bmatrix}, \quad (18)$$

where the first block column/row is size  $dn$  and corresponds to the rotational variables  $R_i$ , the second block column/row is size  $l$  and corresponds to the auxiliary distance variables  $r_{ij}$ , and the last block column/row is size  $n$  and corresponds to the translational states  $t_i$ .

The block matrices which make up  $Q_p$  are the same matrices defined in [8], which connect the estimation problem to the underlying graphical structure. Similarly, the block matrices which form  $Q_r$  are identical to the matrices defined in [45] and also draw on the graphical structure of the underlying inference problem.

### APPENDIX C DEFINING THE CONSTRAINTS, $A_i$

We define the constraints  $\text{tr}(A_i XX^\top) = b_i$  which arise in the SDP (Problem 3) and rank-restricted SDP (Problem 4) problems. Each constraint is defined by a matrix-scalar pair,  $(A_i, b_i)$ , where  $A_i \in \mathbb{R}^{k \times k}$  is a real, symmetric matrix and  $b_i \in \mathbb{R}$  is a scalar.

The constraints can be sorted as either orthonormality constraints,  $R_i^\top R_i = I_d$ , or unit-norm constraints,  $\|r_{ij}\|_2^2 = 1$ . As described in Section IV-A, each orthonormality constraint

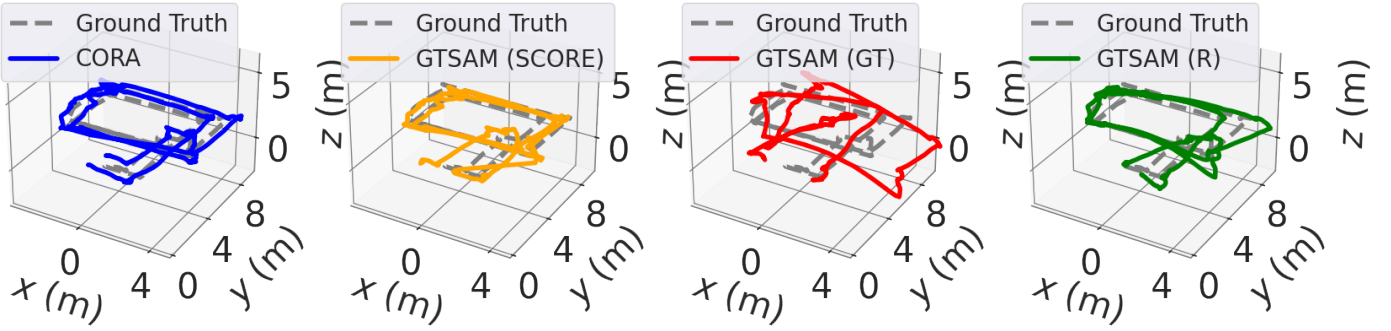


Fig. 6. **Estimated Drone Trajectories:** the trajectory estimates obtained from the drone experiment, with the ground truth shown (grey). It is seen that CORA (blue) obtains a qualitatively more correct trajectory than any of the baseline methods. This is supported by the error statistics shown in Table II.

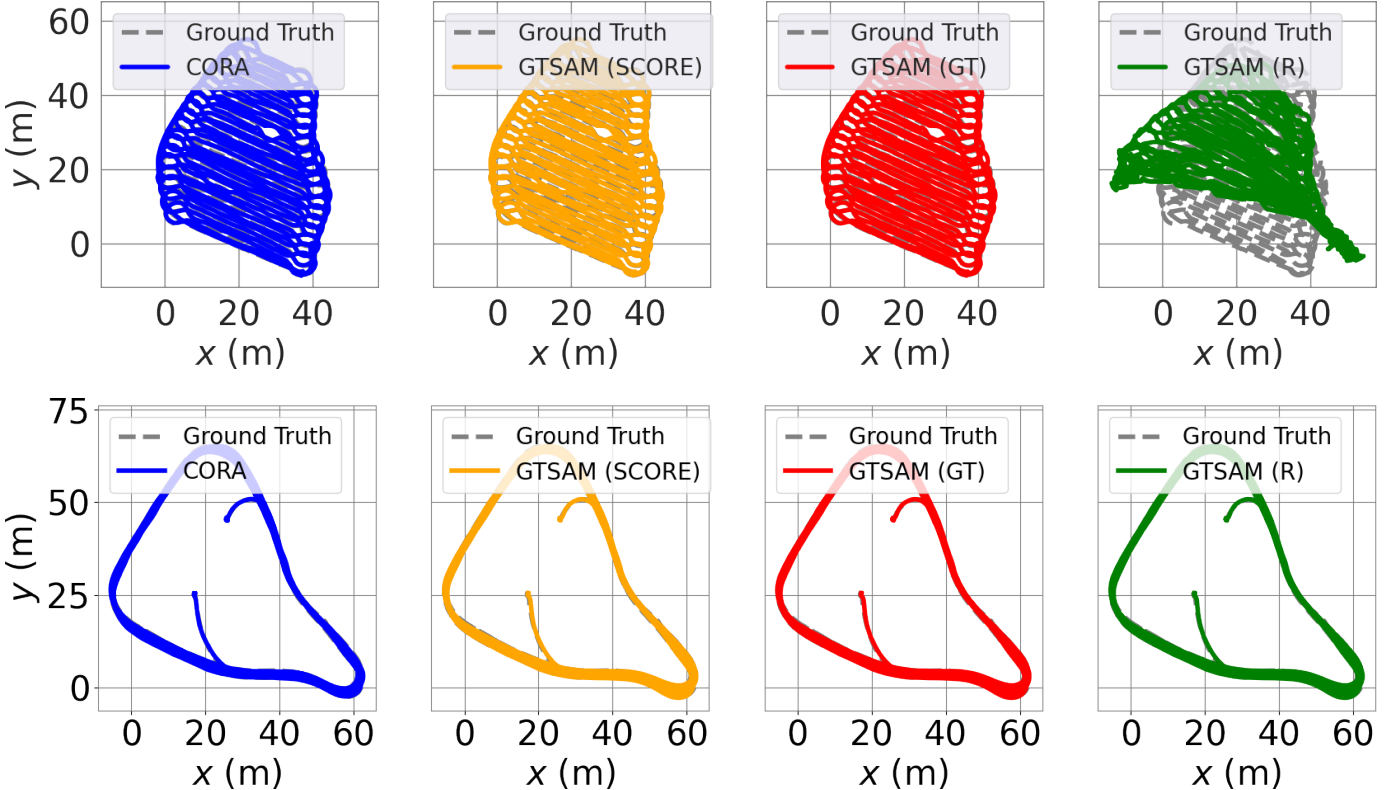


Fig. 7. **Estimated Plaza Trajectories:** the trajectory estimates obtained from the Plaza 1 (Top) and Plaza 2 (Bottom) data sets. The ground truth is shown in grey. CORA with a random initialization (blue) obtains an estimate which is qualitatively similar to the GTSAM estimates initialized with SCORE (yellow) and ground truth beacon positions (red). The GTSAM estimate initialized with random beacon positions (green) was clearly suboptimal for the Plaza 1 data set, did appear to converge to the correct solution for the Plaza 2 data set.

is  $\frac{d(d+1)}{2}$  constraints in the form of  $\text{tr}(A_i X X^\top) = b_i$  and as each unit-norm constraint is a single constraint in the same form.

Each constraint  $A_i$  is has a block-diagonal sparsity pattern and is nonzero only in the block entry corresponding to the variable it constrains.

### Orthonormality Constraints

As they correspond to  $R_i$  variables, the orthonormality constraints occupy the upper-left  $n$  ( $d \times d$ ) block-diagonal entries of the constraint matrices. As  $R_i^\top R_i$  is symmetric, it suffices to explicitly constrain only the upper-triangular entries of  $R_i^\top R_i$ . The constraint  $A_{j,k,l}$  denotes the constraint corresponding to the  $(k, l)$  entry of  $R_i^\top R_j$ . We can write  $A_{j,k,l}$

$$A_{j,k,l} \triangleq \begin{bmatrix} 0 & & & \\ & \ddots & & \\ & & \overline{A}_{j,k,l} & \\ & & & \ddots & \\ & & & & 0 \end{bmatrix} \quad (19)$$

where  $\overline{A}_{j,k,l}$  is in the  $j$ th  $(d \times d)$  block-diagonal entry.

In the case that  $k \neq l$ , the  $(p, q)$  entry of  $\overline{A}_{j,k,l}$  is defined as:

$$\overline{A}_{j,k,l}(p,q) \triangleq \begin{cases} 1/2 & \text{if } (p,q) = (k,l) \\ 1/2 & \text{if } (p,q) = (l,k) \\ 0 & \text{otherwise} \end{cases} \quad (20)$$

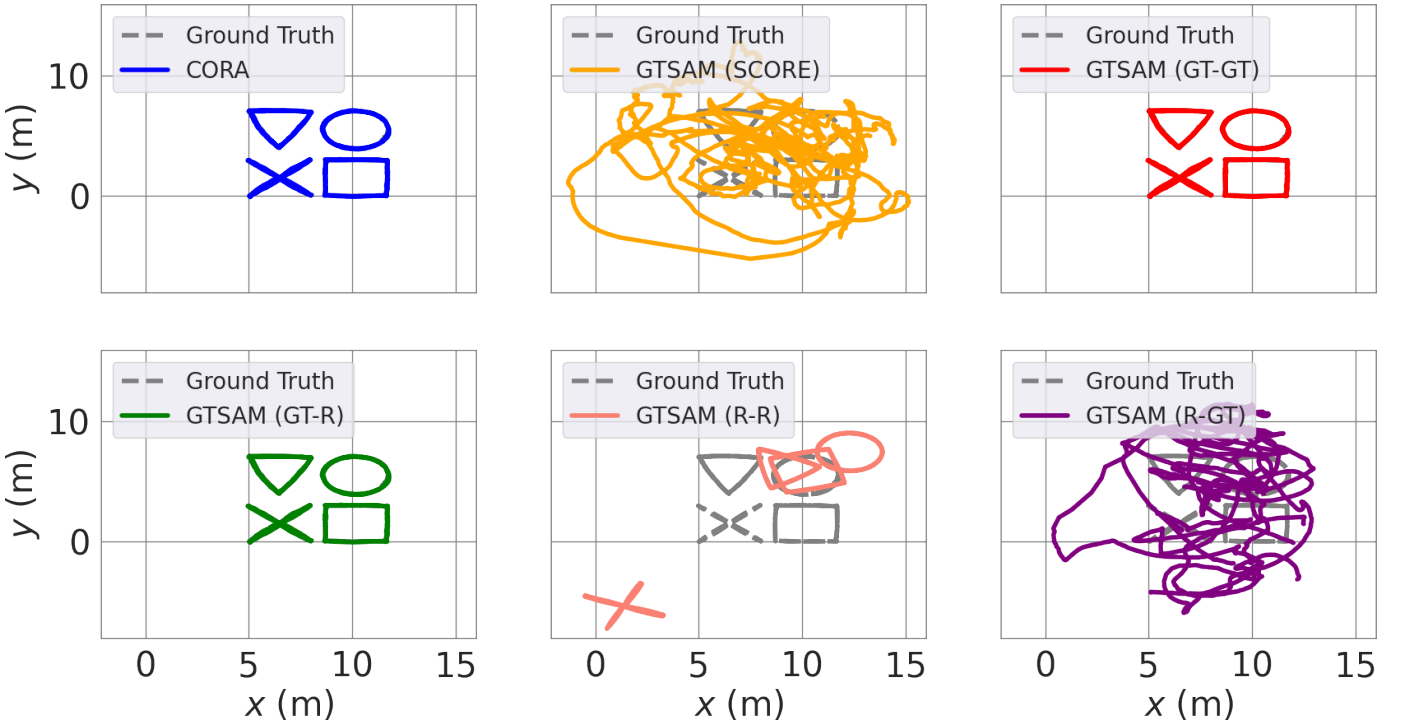


Fig. 8. **Estimated Tiers Trajectories:** the trajectory estimates obtained from the Tiers dataset [73]. The ground truth is shown in grey. CORA obtains a qualitatively correct result which is the same as the baselines in which the solution is initialized by ground truth starting poses (GT-GT and GT-R). In contrast, the remaining baselines (SCORE, R-R, and R-GT) obtained clearly sub-optimal solutions. These results suggest the fragility of existing methods in which the initial poses are not known, and the value of the initialization-independent results from CORA.

with corresponding scalar  $b_{j,k,l} = 0$ .

In the case that  $k = l$ , the  $(p, q)$  entry of  $\bar{A}_{j,k,l}$  is defined as:

$$\bar{A}_{j,k,l}(p, q) \triangleq \begin{cases} 1 & \text{if } (p, q) = (k, k) \\ 0 & \text{otherwise} \end{cases} \quad (21)$$

with corresponding scalar  $b_{j,k,l} = 1$ .

#### Unit-Norm Constraints

The unit-norm constraints exist in the  $l$  diagonal entries following the first  $n$  ( $d \times d$ ) block-diagonal entries. We number the  $r_{ij}$  variables in the order they appear as:  $r_1, r_2$ , etcetera. The constraint  $A_{r_l}$  corresponding the  $l$ th distance variable,  $r_l$  is defined as:

$$A_{r_{ij}} \triangleq \text{diag}(0_{dn}, 0_{l-1}, 1, 0_{k-(l+dn+1)}) \in \mathbb{R}^{k \times k} \quad (22)$$

where  $0_v$  indicates a vector of  $v$  zeros,  $\text{diag}(\cdot)$  indicates the mapping from a vector to a diagonal matrix, and  $k \triangleq (d+1)n + l$  is the height of the matrix  $X$ .

#### APPENDIX D PRECONDITIONING

In this section we provide a brief overview of preconditioning and describe the preconditioner designed for CORA.

The convergence of conjugate gradients to solve the problem  $Ax = b$  is highly dependent on the condition number  $\kappa(A) \triangleq \frac{\lambda_{\max}(A)}{\lambda_{\min}(A)}$ , as defined as the ratio of the largest eigenvalue to the smallest eigenvalue of  $A$  [70, Section 10.3].

The convergence can be improved by preconditioning the problem with a matrix  $P$  such that  $\kappa(P^{-1}A) \ll \kappa(A)$ . The (equivalent) preconditioned problem is then  $P^{-1}Ax = P^{-1}b$ .

The optimal preconditioner  $P$  is the inverse of the matrix  $A$ , however computing the exact inverse is equivalent to solving the original problem. Thus, approximate preconditioners, which can be computed efficiently, are used in practice; preconditioning strategies trade off the accuracy of the preconditioner with the computational cost of computing the preconditioner. Several common preconditioning strategies are the Jacobi preconditioner and its block variant, the incomplete Cholesky preconditioner, and the regularized incomplete Cholesky preconditioner [76, Chapter 10].

#### Block-Diagonal Cholesky Preconditioner

Whereas these preconditioners are designed for general systems, we design a block-diagonal Cholesky preconditioner which leverages the structure of the data matrix  $Q$ .

Recall from Appendix B that  $Q$  takes the form of:

$$Q = \begin{bmatrix} L(G^\rho) + \Sigma & 0 & \tilde{V} \\ 0 & W\tilde{D}^2 & C^\top W\tilde{D} \\ \tilde{V}^\top & \tilde{D}WC & C^\top WC + L(G^\tau) \end{bmatrix}. \quad (23)$$

We leverage the block-structure of  $Q$  to design a preconditioner. Specifically, we strictly consider the block-diagonal approximation of  $Q$ ,

$$\tilde{Q} = \begin{bmatrix} L(G^\rho) + \Sigma & 0 & 0 \\ 0 & W\tilde{D}^2 & 0 \\ 0 & 0 & C^\top WC + L(G^\tau) \end{bmatrix}. \quad (24)$$

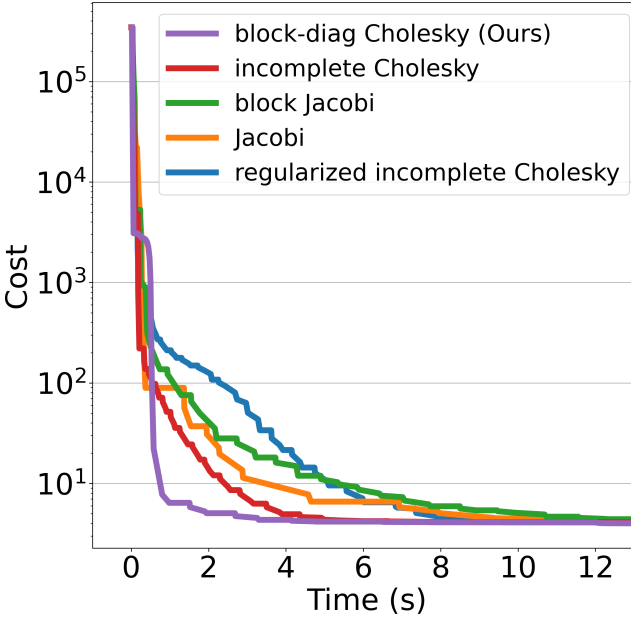


Fig. 9. **Solver cost over time:** the cost at a given iterate of the Riemannian Trust Region optimizer compared to the time spent in the optimizer up to that point. The figure compares each preconditioner in the single-drone experiment (Section VII-A1). The figure zooms in on the first 13 seconds to highlight the initial difference in convergence between the proposed block diagonal Cholesky preconditioner and the other preconditioners.

This approximation has the advantage of being block-diagonal, which allows us to compute the inverse of  $\tilde{Q}$  by inverting each block separately. Additionally,  $Q$  is typically block-diagonally dominant due to graphical structure of the problem [8, 45], meaning that  $\tilde{Q}$  preserves much of the structure of  $Q$ . Furthermore, these blocks are highly sparse, again due to the graphical structure of the problem. This lends substantial computational efficiency to both the inversion of  $\tilde{Q}$  and application of the preconditioner.

To efficiently compute the inverse of the first block,  $L(G^\rho) + \Sigma$ , we compute its Cholesky decomposition and use the resulting factorization to apply the inverse. The second block,  $W\tilde{D}^2$ , is a diagonal matrix and thus is trivially inverted.

The third block,  $C^\top WC + L(G^\tau)$ , is notably the sum of two graph Laplacians and thus is singular. This is due to the fact that graph Laplacians have a nullspace which contains the all-ones vector. In our problem this nullspace can be interpreted as the fact that the cost is identical up to a translational offset, that is the estimated translations can be identically shifted without incurring additional cost.

The existence of this nullspace means that the matrix  $C^\top WC + L(G^\tau)$  is singular and thus cannot be inverted. However, we can ‘pin’ the Laplacians by removing a single row and corresponding column. This can be considered equivalent to fixing the translational offset of the estimated trajectories [43]. Without loss of generality we choose to remove the last row and column of  $C^\top WC + L(G^\tau)$ ; from this point we can compute the Cholesky decomposition of the resulting matrix and use the resulting factorization to apply the inverse.

We denote the ‘pinned’ matrix as  $\underline{L}_{tran}$ . To account for the ‘pinned’ translational state when applying  $\underline{L}_{tran}^{-1}x$  as a preconditioner to  $x$  we ignore the last row of  $x$  when applying

Preconditioner	Single Drone	Plaza 1	Plaza 2	TIERS
<b>Ours</b>	<b>23 (s)</b>	<b>26 (s)</b>	<b>4 (s)</b>	<b>29 (s)</b>
inc. Cholesky	44 (s)	76 (s)	14 (s)	229 (s)
block Jacobi	54 (s)	178 (s)	20 (s)	1468 (s)
Jacobi	54 (s)	207 (s)	41 (s)	927 (s)
reg. inc. Cholesky	47 (s)	242 (s)	28 (s)	703 (s)

TABLE VI  
PRECONDITIONER PERFORMANCE: THE TIME SPENT IN THE RIEMANNIAN TRUST REGION SOLVER FOR EACH PRECONDITIONER ON ALL OF THE REAL-WORLD EXPERIMENTS FROM SECTION VII-A.

$\underline{L}_{tran}^{-1}$  and pad the result with zeros. This corresponds to pinning the translational offset at the origin.

We have established that our preconditioner  $P$  consists of Cholesky decompositions of the first and third blocks of  $\tilde{Q}$  and the inverse of the second block of  $\tilde{Q}$ :

$$R_r^\top R_r = L(G^\rho) + \Sigma \quad (25)$$

$$R_t^\top R_t = \underline{L}_{tran} \quad (26)$$

$$P = \begin{bmatrix} (R_r^\top R_r)^{-1} & 0 & 0 \\ 0 & W^{-1}\tilde{D}^{-2} & 0 \\ 0 & 0 & (R_t^\top R_t)^{-1} \end{bmatrix}. \quad (27)$$

We note that, for computational reasons, we never explicitly compute the preconditioner  $P$ ; the blocks of  $P$  are generically dense and thus expensive to store and apply. Instead, we store the Cholesky factors and apply their inverses via forward- and back-substitution.

### Evaluation

We evaluate the performance of our preconditioner against the standard preconditioners mentioned above: the Jacobi, block-Jacobi, incomplete Cholesky, and regularized incomplete Cholesky preconditioners. As different preconditioners may be cheaper to apply but result in slower convergence, we evaluate the preconditioners in terms of the time spent in the Riemannian trust region solver.

This is not the total time CORA spends solving each problem, as this neglects the time spent in certification and saddle escape. This timing methodology provides a clearer picture of the effect of the preconditioner on runtime.

We test each preconditioner on the real-world problems from Section VII-A with identical parameters. All problems are initialized with robot odometry, the first pose of each robot is given as ground truth, and the positions of all beacons are initialized at their ground truth values.

We show the solver cost over time for the single-drone experiment in Fig. 9. It can be seen that the proposed block-diagonal Cholesky preconditioner obtains a lower cost much more quickly than the other preconditioners. The trends shown in Fig. 9 were found to be consistent across all experiments.

The timing results for all experiments are shown in Table VI. For each experiment the block-diagonal Cholesky preconditioner we designed for CORA obtains solutions 2-10 times faster than the next fastest preconditioner.

## REFERENCES

- [1] Jesse R. Pelletier, Brendan W. O'Neill, John J. Leonard, Lee Freitag, and Eric Gallimore. AUV-assisted diver navigation. *IEEE Robotics and Automation Letters*, 7(4):10208–10215, 2022. ISSN 23773766. doi: 10.1109/LRA.2022.3191164.
- [2] Liam Paull, Sajad Saeedi, Mae Seto, and Howard Li. AUV navigation and localization: A review. *Oceanic Engineering, IEEE Journal of*, 39(1):131–149, 2014.
- [3] Kexin Guo, Zhirong Qiu, Wei Meng, Lihua Xie, and Rodney Teo. Ultra-wideband based cooperative relative localization algorithm and experiments for multiple unmanned aerial vehicles in GPS denied environments. *International Journal of Micro Air Vehicles*, 9(3):169–186, 2017. ISSN 17568307. doi: 10.1177/1756829317695564.
- [4] Nobuhiro Funabiki, Benjamin Morrell, Jeremy Nash, and Ali Akbar Agha-Mohammadi. Range-aided pose-graph-based SLAM: Applications of deployable ranging beacons for unknown environment exploration. *IEEE Robotics and Automation Letters*, 6(1):48–55, 2021. ISSN 23773766. doi: 10.1109/LRA.2020.3026659.
- [5] Elizabeth R Boroson, Robert Hewitt, Nora Ayanian, and Jean-pierre De Croix. Inter-robot range measurements in pose graph optimization. *2020 IEEE/RSJ International Conference on Intelligent Robots and Systems (IROS)*, pages 4806–4813, 2020.
- [6] C. D. Cadena Lerma, L. Carlone, H. Carrillo, Y. Latif, D. Scaramuzza, J. Neira, I. Reid, and J. Leonard. Past, present, and future of simultaneous localization and mapping: Towards the robust-perception age. *IEEE Trans. Robotics*, 2016.
- [7] David M. Rosen, Kevin J. Doherty, Antonio Terán Espinoza, and John J. Leonard. Advances in inference and representation for simultaneous localization and mapping. *Annual Review of Control, Robotics, and Autonomous Systems*, 4(1):215–242, 2021. ISSN 2573-5144. doi: 10.1146/annurev-control-072720-082553.
- [8] David M. Rosen, Luca Carlone, Afonso S. Bandeira, and John J. Leonard. SE-Sync: A certifiably correct algorithm for synchronization over the special Euclidean group. *The International Journal of Robotics Research*, 38(2-3):95–125, 2019. ISSN 17413176. doi: 10.1177/0278364918784361.
- [9] F. Dellaert and M. Kaess. Square Root SAM: Simultaneous localization and mapping via square root information smoothing. *Intl. J. of Robotics Research*, 25(12):1181–1203, December 2006.
- [10] M. Kaess, A. Ranganathan, and F. Dellaert. iSAM: Incremental smoothing and mapping. *IEEE Trans. Robotics*, 24(6):1365–1378, December 2008.
- [11] Naum Z Shor. Quadratic optimization problems. *Soviet Journal of Computer and Systems Sciences*, 25:1–11, 1987.
- [12] Nicolas Boumal. A Riemannian low-rank method for optimization over semidefinite matrices with block-diagonal constraints. pages 1–36, 2015. URL <http://arxiv.org/abs/1506.00575>.
- [13] Nicolas Boumal, Vladislav Voroninski, and Afonso S. Bandeira. The non-convex Burer-Monteiro approach works on smooth semidefinite programs. *Advances in Neural Information Processing Systems*, (Nips):2765–2773, 2016. ISSN 10495258.
- [14] Samuel Burer and Renato DC Monteiro. A nonlinear programming algorithm for solving semidefinite programs via low-rank factorization. *Mathematical Programming*, 95(2):329–357, 2003.
- [15] Timothy D Barfoot. *State Estimation for Robotics*. Cambridge University Press, 2017.
- [16] Afonso S Bandeira. A note on probably certifiably correct algorithms. *Comptes Rendus Mathematique*, 354(3):329–333, 2016.
- [17] David M. Rosen. Scalable low-rank semidefinite programming for certifiably correct machine perception. pages 551–566, 2020. ISSN 25111264. doi: 10.1007/978-3-030-66723-8\_33.
- [18] V. Jeyakumar, A. M. Rubinov, and Z. Y. Wu. Non-convex quadratic minimization problems with quadratic constraints: Global optimality conditions. *Mathematical Programming*, 110(3):521–541, 2007. ISSN 00255610. doi: 10.1007/s10107-006-0012-5.
- [19] Guoyin Li. Global quadratic minimization over bivalent constraints: Necessary and sufficient global optimality condition. *Journal of Optimization Theory and Applications*, 152(3):710–726, 2012. ISSN 15732878. doi: 10.1007/s10957-011-9930-3.
- [20] Yulun Tian, Kasra Khosoussi, David M Rosen, and Jonathan P How. Distributed certifiably correct pose-graph optimization. *IEEE Transactions on Robotics*, 37(6):2137–2156, 2021.
- [21] José Pedro Iglesias, Carl Olsson, and Fredrik Kahl. Global optimality for point set registration using semidefinite programming. *Proceedings of the IEEE Computer Society Conference on Computer Vision and Pattern Recognition*, pages 8284–8292, 2020. ISSN 10636919. doi: 10.1109/CVPR42600.2020.00831.
- [22] Heng Yang, Jingnan Shi, and Luca Carlone. TEASER: Fast and certifiable point cloud registration. *IEEE Transactions on Robotics*, pages 1–44, 2020. ISSN 19410468. doi: 10.1109/TRO.2020.3033695.
- [23] Mercedes Garcia-Salguero, Jesus Briales, and Javier Gonzalez-Jimenez. Certifiable relative pose estimation. *Image and Vision Computing*, 109, 2021. ISSN 02628856. doi: 10.1016/j.imavis.2021.104142.
- [24] Jesus Briales and Javier Gonzalez-Jimenez. Fast global optimality verification in 3D SLAM. *IEEE International Conference on Intelligent Robots and Systems*, pages 4630–4636, 2016. ISSN 21530866. doi: 10.1109/IROS.2016.7759681.
- [25] Luca Carlone, David M. Rosen, Giuseppe Calafiore, John J. Leonard, and Frank Dellaert. Lagrangian duality in 3D SLAM: Verification techniques and optimal solutions. *IEEE International Conference on Intelligent Robots and Systems*, 2015-Decem:125–132, 2015. ISSN 21530866. doi: 10.1109/IROS.2015.7353364.
- [26] Frederike Dümbgen, Connor Holmes, and Timothy D.

Barfoot. Safe and smooth: Certified continuous-time range-only localization. *IEEE Robotics and Automation Letters*, 2022. URL <http://arxiv.org/abs/2209.04266>.

[27] Mercedes Garcia-Salguero and Javier Gonzalez-Jimenez. A sufficient condition of optimality for the relative pose problem between cameras. *SIAM Journal on Imaging Sciences*, 14(4):1617–1634, 2021. doi: 10.1137/21m1397970.

[28] Richard Hartley, Fredrik Kahl, Carl Olsson, and Yongduak Seo. Verifying global minima for L2 minimization problems in multiple view geometry. *International Journal of Computer Vision*, 101(2):288–304, 2013. ISSN 09205691. doi: 10.1007/s11263-012-0569-9.

[29] Carl Olsson, Fredrik Kahl, and Richard Hartley. Projective least-squares: Global solutions with local optimization. *2009 IEEE Conference on Computer Vision and Pattern Recognition, CVPR 2009*, pages 1216–1223, 2009. doi: 10.1109/CVPRW.2009.5206864.

[30] Xiaowei Bao, Nikolaos V. Sahinidis, and Mohit Tawar-malani. Semidefinite relaxations for quadratically constrained quadratic programming: A review and comparisons. *Mathematical Programming*, 129(1):129–157, 2011. ISSN 00255610. doi: 10.1007/s10107-011-0462-2.

[31] Jesus Briales and Javier Gonzalez-Jimenez. Convex global 3D registration with Lagrangian duality. *Proceedings - 30th IEEE Conference on Computer Vision and Pattern Recognition, CVPR 2017*, 2017-Janua:5612–5621, 2017. doi: 10.1109/CVPR.2017.595.

[32] Carl Olsson and Anders Eriksson. Solving quadratically constrained geometrical problems using Lagrangian duality. *Proceedings - International Conference on Pattern Recognition*, 2008. ISSN 10514651. doi: 10.1109/icpr.2008.4761896.

[33] Yuehaw Khoo and Ankur Kapoor. Non-iterative rigid 2D/3D point-set registration using semidefinite programming. *IEEE Transactions on Image Processing*, 25(7):2956–2970, 2016. ISSN 10577149. doi: 10.1109/TIP.2016.2540810.

[34] Heng Yang and Luca Carlone. A polynomial-time solution for robust registration with extreme outlier rates. *Robotics: Science and Systems*, (Section IV), 2019. ISSN 2330765X. doi: 10.15607/RSS.2019.XV.003.

[35] Jesus Briales, Laurent Kneip, and Javier Gonzalez-Jimenez. A certifiably globally optimal solution to the non-minimal relative pose problem. In *Proceedings of the IEEE Computer Society Conference on Computer Vision and Pattern Recognition*, pages 145–154, 2018. ISBN 9781538664209. doi: 10.1109/CVPR.2018.00023.

[36] Mercedes Garcia-Salguero, Jesus Briales, and Javier Gonzalez-Jimenez. A tighter relaxation for the relative pose problem between cameras. *Journal of Mathematical Imaging and Vision*, 64(5):493–505, 2022. ISSN 15737683. doi: 10.1007/s10851-022-01085-z. URL <https://doi.org/10.1007/s10851-022-01085-z>.

[37] Chris Aholt, Sameer Agarwal, and Rekha Thomas. A QCQP approach to triangulation. *Lecture Notes in Computer Science (including subseries Lecture Notes in Artificial Intelligence and Lecture Notes in Bioinformatics)*, 7572 LNCS(PART 1):654–667, 2012. ISSN 03029743. doi: 10.1007/978-3-642-33718-5\_47.

[38] Yingjian Wang, Xiangyong Wen, Longji Yin, Chao Xu, Yanjun Cao, and Fei Gao. Certifiably optimal mutual localization with anonymous bearing measurements.

[39] Ji Zhao. An efficient solution to non-minimal case essential matrix estimation. *IEEE Transactions on Pattern Analysis and Machine Intelligence*, 44(4):1–1, 2020. ISSN 0162-8828. doi: 10.1109/tpami.2020.3030161.

[40] Luca Carlone, Giuseppe C. Calafiore, Carlo Tommollo, and Frank Dellaert. Planar pose graph optimization: Duality, optimal solutions, and verification. *IEEE Transactions on Robotics*, 32(3):545–565, 2016. ISSN 15523098. doi: 10.1109/TRO.2016.2544304.

[41] Matthew Giamou, Ziye Ma, Valentin Peretroukhin, and Jonathan Kelly. Certifiably globally optimal extrinsic calibration from per-sensor egomotion. *IEEE Robotics and Automation Letters*, 4(2):367–374, 2019. ISSN 23773766. doi: 10.1109/LRA.2018.2890444Y.

[42] Samuel Burer and Renato DC Monteiro. Local minima and convergence in low-rank semidefinite programming. *Mathematical programming*, 103(3):427–444, 2005.

[43] Jesus Briales and Javier Gonzalez-Jimenez. Cartan-sync: Fast and global SE(d)-synchronization. *IEEE Robotics and Automation Letters*, 2(4):2127–2134, 2017. ISSN 23773766. doi: 10.1109/LRA.2017.2718661.

[44] Taosha Fan, Hanlin Wang, Michael Rubenstein, and Todd Murphy. CPL-SLAM: Efficient and certifiably correct planar graph-based SLAM using the complex number representation. *IEEE Transactions on Robotics*, 36:1719–1737, 2020. URL <http://arxiv.org/abs/2007.06708>.

[45] Trevor Halsted and Mac Schwager. The Riemannian elevator for certifiable distance-based localization. *Preprint*, 2022. Accessed: Jan. 20, 2023. [Online] Available [https://msl.stanford.edu/papers/halsted\\_riemannian\\_2022.pdf](https://msl.stanford.edu/papers/halsted_riemannian_2022.pdf).

[46] David R Morrison, Sheldon H Jacobson, Jason J Sauppe, and Edward C Sewell. Branch-and-bound algorithms: A survey of recent advances in searching, branching, and pruning. *Discrete Optimization*, 19:79–102, 2016.

[47] David Cox, John Little, and Donal OShea. *Ideals, varieties, and algorithms: an introduction to computational algebraic geometry and commutative algebra*. Springer Science & Business Media, 2013.

[48] Faraz M. Mirzaei and Stergios I. Roumeliotis. Optimal estimation of vanishing points in a Manhattan world. *Proceedings of the IEEE International Conference on Computer Vision*, pages 2454–2461, 2011. doi: 10.1109/ICCV.2011.6126530.

[49] Henrik Stewénus, Frederik Schaffalitzky, and David Nistér. How hard is 3-view triangulation really? *Proceedings of the IEEE International Conference on Computer Vision*, 1:686–693, 2005. doi: 10.1109/ICCV.2005.115.

[50] Nikolas Trawny and Stergios I Roumeliotis. On the global optimum of planar, range-based robot-to-robot relative pose estimation. In *2010 IEEE International Conference on Robotics and Automation*, pages 3200–

3206. IEEE, 2010.

[51] Faraz M. Mirzaei and Stergios I. Roumeliotis. Globally optimal pose estimation from line correspondences. *Proceedings - IEEE International Conference on Robotics and Automation*, pages 5581–5588, 2011. ISSN 10504729. doi: 10.1109/ICRA.2011.5980272.

[52] Jean-Charles Bazin, Yongduek Seo, and Marc Pollefeys. Globally optimal consensus set maximization through rotation search. In *Asian Conference on Computer Vision*, pages 539–551. Springer, 2012.

[53] Carl Olsson, Fredrik Kahl, and Magnus Oskarsson. Branch-and-bound methods for Euclidean registration problems. *IEEE Transactions on Pattern Analysis and Machine Intelligence*, 31(5):783–794, 2009. ISSN 01628828. doi: 10.1109/TPAMI.2008.131.

[54] Gregory Izatt, Hongkai Dai, and Russ Tedrake. Globally optimal object pose estimation in point clouds with mixed-integer programming. *Springer Proceedings in Advanced Robotics*, 10:695–710, 2020. ISSN 25111264. doi: 10.1007/978-3-030-28619-4\_49.

[55] Jiaolong Yang, Hongdong Li, Dylan Campbell, and Yunde Jia. Go-ICP: A globally optimal solution to 3D ICP point-set registration. *IEEE Transactions on Pattern Analysis and Machine Intelligence*, 38(11):2241–2254, 2016. ISSN 01628828. doi: 10.1109/TPAMI.2015.2513405.

[56] Jean-Charles Bazin, Yongduek Seo, Richard Hartley, and Marc Pollefeys. Globally optimal inlier set maximization with unknown rotation and focal length. In *European Conference on Computer Vision*, pages 803–817. Springer, 2014.

[57] Dylan Campbell, Lars Petersson, Laurent Kneip, and Hongdong Li. Globally-optimal inlier set maximisation for simultaneous camera pose and feature correspondence. In *Proceedings of the IEEE International Conference on Computer Vision*, pages 1–10, 2017.

[58] Johan Fredriksson, Viktor Larsson, Carl Olsson, and Fredrik Kahl. Optimal relative pose with unknown correspondences. *Proceedings of the IEEE Computer Society Conference on Computer Vision and Pattern Recognition*, 2016-Decem:1728–1736, 2016. ISSN 10636919. doi: 10.1109/CVPR.2016.191.

[59] Richard I. Hartley and Fredrik Kahl. Global optimization through rotation space search. *International Journal of Computer Vision*, 82(1):64–79, 2009. ISSN 15731405. doi: 10.1007/s11263-008-0186-9.

[60] Laurent Kneip and Simon Lynen. Direct optimization of frame-to-frame rotation. *Proceedings of the IEEE International Conference on Computer Vision*, pages 2352–2359, 2013. doi: 10.1109/ICCV.2013.292.

[61] Fangfang Lu and Richard Hartley. A fast optimal algorithm for L2 triangulation. *Lecture Notes in Computer Science (including subseries Lecture Notes in Artificial Intelligence and Lecture Notes in Bioinformatics)*, 4844 LNCS(PART 2):279–288, 2007. ISSN 16113349. doi: 10.1007/978-3-540-76390-1\_28.

[62] Alessandro Chiuso, Giorgio Picci, and Stefano Soatto. Wide-sense estimation on the special orthogonal group. *Communications in Information and Systems*, 8(3):185–200, 2008. ISSN 15267555. doi: 10.4310/cis.2008.v8.n3.a1.

[63] Alan Papalia, Joseph Morales, Kevin J. Doherty, David M. Rosen, and John J. Leonard. SCORE: A second-order conic initialization for range-aided SLAM. In *2023 IEEE International Conference on Robotics and Automation (ICRA)*, pages 10637–10644. IEEE, 2023.

[64] Roberto Tron, David M Rosen, and Luca Carlone. On the inclusion of determinant constraints in lagrangian duality for 3d slam. *Proc. Robotics: Science and Systems (RSS), Workshop "The Problem of Mobile Sensors"*, 2(1), 2015.

[65] Gerd Wachsmuth. On LICQ and the uniqueness of Lagrange multipliers. *Operations Research Letters*, 41(1):78–80, 2013.

[66] Nicolas Boumal. *An Introduction to Optimization on Smooth Manifolds*. Cambridge University Press, 2023.

[67] Jorge Nocedal and Stephen Wright. *Numerical optimization*. Springer, 1999.

[68] David M Rosen. Accelerating certifiable estimation with preconditioned eigensolvers. *IEEE Robotics and Automation Letters*, 2022.

[69] Pierre-Antoine Absil, Christopher G. Baker, and Kyle A. Gallivan. Trust-region methods on riemannian manifolds. *Foundations of Computational Mathematics*, 7:303–330, 2007.

[70] G. Golub and C. Van Loan. *Matrix Computations*. Johns Hopkins University Press, Baltimore, MD, 3rd edition, 1996.

[71] Frank Dellaert and GTSAM Contributors. borglab/gtsam, May 2022. URL <https://github.com/borglab/gtsam>.

[72] Joseph Djugash and Stephan Roth. Navigating with ranging radios: Five data sets with ground truth. *Journal of Field Robotics*, 26(9):689–695, 2009. doi: 10.1002/rob.21514. URL <http://onlinelibrary.wiley.com/doi/10.1002/rob.21514/abstract>.

[73] Xianjia Yu, Paola Torrico Morrn, Sahar Salimpour, Jorge Pena Queralta, and Tomi Westerlund. Loosely coupled odometry, uwb ranging, and cooperative spatial detection for relative monte-carlo multi-robot localization. *arXiv preprint arXiv:2304.06264*, 2023.

[74] Michael Grupp. evo: Python package for the evaluation of odometry and slam. <https://github.com/MichaelGrupp/evo>, 2017.

[75] Antoni Rosinol, Marcus Abate, Yun Chang, and Luca Carlone. Kimera: an open-source library for real-time metric-semantic localization and mapping. In *2020 IEEE International Conference on Robotics and Automation (ICRA)*, pages 1689–1696. IEEE, 2020.

[76] Yousef Saad. *Iterative methods for sparse linear systems*. SIAM, 2003.